Universität Zürich[UZH]

Geographisches Institut

# Evaluating the Suitability of Spectral Indices and Functional Diversity Metrics for Biodiversity Monitoring in West Kalimantan, Borneo

GEO 511 Master's Thesis

**Author:** Nathalie Nitsingam, 18-926-378

**Supervised by:** Jochem Braakhekke, Dr. Isabelle Helfenstein, Dr. Claudia Röösli

**Faculty representative:** Prof. Dr. Maria J. Santos

30.11.2025

Universität Zürich[UZH]

# Evaluating the Suitability of Spectral Indices and Functional Diversity Metrics for Biodiversity Monitoring in West Kalimantan, Borneo

GEO 511 Master's Thesis


**Student**

Nathalie Nitsingam

18-926-378

**Supervised by**

Jochem Braakhekke

Dr. Isabelle Helfenstein

Dr. Claudia Röösli

**Faculty Representative**

Prof. Dr. Maria J. Sanchez


30.11.2025


Department of Geography, University of Zurich

# Abstract

Borneo is one of the world's most valuable biodiversity hotspots but faces increasing pressure from land conversion, particularly the expansion of oil-palm plantations. More sustainable systems such as agroforestry are being established, yet it requires monitoring approaches that are scalable, accessible, and cost-effective in order to be able to track the progress of such systems. Remote sensing offers such opportunities by enabling the estimation of functional traits and functional diversity across large areas and long time series, although high cloud cover remains a major challenge in tropical regions.

This thesis evaluates the potential and limitations of Sentinel-2 vegetation indices and functional diversity metrics for long-term monitoring across natural forest, agroforestry, and oil-palm plantations in West Kalimantan, Borneo. Cloud masking was applied to Sentinel-2 data from 2019–2024 in order to increase the number of observations per sample site, as fully cloud-free images are rare in tropical forest ecosystems. Nineteen spectral indices describing chlorophyll, water, and pigment traits were analyzed for temporal patterns and differences between land-cover types. Seventeen indices showed a significant correlation with cloud-cover probability (10 weak, 7 moderate), indicating potential bias from residual cloud effects. All indices differed significantly between land-cover types. Fifteen indices were significantly related to dry and wet seasons and showed seasonal patterns, that indicate the presence of dry-season greening similar to observations in other tropical forests. These findings highlight the need to consider seasonality when designing monitoring intervals.

Based on their strong discrimination between land-cover types and low correlation with cloud-cover probability, NDRE2, NDII, and PSRI were selected to calculate Functional Richness (FRic) and Functional Divergence (FDiv). FDiv aligned well with ecological expectations and showed neither a trend nor a seasonality. FRic was strongly affected by plot size and mixed-pixel effects, inflating values in agroforestry plots. Overall, the results show that Sentinel-2 can support functional-trait-based biodiversity monitoring in tropical systems, provided that cloud masking, index choice, and spatial scale are carefully considered.

# Acknowledgements

First of all, I want to thank my supervisors Jochem Braakhekke and Dr. Isabelle Helfenstein for their feedback, encouragement and for all their patience throughout the whole thesis. I really appreciate the time they took for discussion and advice. I also want to thank Dr. Claudia Röösli for her constructive feedback and helpful input during different stages of this work.

Special thanks go to Dr. Emina Besic Gyenge and Dirk-Jan Oudshoorn from Rahn and Forestwise for making this thesis possible, providing data and sharing insights into their project. Working on this thesis offered be a very interesting insight into the topic of agroforestry. I also want to thank Emina and Rahn for making it possible for me to attend the Living Planet Symposium, which was an inspiring and very memorable experience.

# Contents

# List of Figures

# List of Tables

# List of Abrevations

| | |
|---|---|
| ARI | Anthocyanin Reflectance Index |
| a.s.l. | Above Sea Level |
| CBD | Convention on Biological Diversity |
| $Cl_{green}$ | Chlorophyll Green Index |
| $Cl_{red\text{-}edge}$ | Chlorophyll Red-Edge Index |
| CRI | Carotenoid Reflectance Index |
| CS+ | Cloud Score+ S2_HARMONIZED V1 |
| EU | European Union |
| FDiv | Functional Divergence |
| FEve | Functional Evenness |
| FRic | Functional Richness |
| FAO | Food and Agricultural Organization |
| GBF | Kunming-Montreal Global Biodiversity Framework |
| GEE | Google Earth Engine |
| GFC2020 | Global Forest Cover Map for the year 2020 |
| LAI | Leaf Area Index |
| MCARI | Modified Chlorophyll Absorption Ratio Index |
| MERIS | Medium Resolution Imaging Spectrometer |
| mARI | Modified Anthocyanin Reflectance Index |
| MSI | Moisture Stress Index |
| n | Sample Size |
| NDII | Normalized Difference Infrared Index |
| NDRE | Normalized Difference Red-Edge Index |
| NDVI | Normalized Difference Vegetation Index |
| NDWI | Normalized Difference Water Index |
| NIR | Near Infrared |
| NMDI | Normalized Moisture Difference Index |
| OSAVI | Optimized Soil-Adjusted Vegetation Index |
| PSRI | Plant Senescence Reflectance Index |

| | |
|---|---|
| Sen2_Harmonized | Harmonized Sentinel-2 MSI: Multispectral Instrument, Level-2A (SR) |
| SR | Simple Ratio |
| Std | Standard Deviation |
| TCARI | Transformed Chlorophyll Absorption Ratio Index |

# 1 Introduction

Biodiversity loss is accelerating worldwide, driven largely by land cover change, climate change, and anthropogenic pressure. Its decline threatens not only the resilience and functioning of ecosystems, but also economic systems and human well-being (Díaz et al., 2006). Even though international concern has sparked decades ago and according agreements attempt to address the crisis, research shows that biodiversity continues to decline at an increasingly alarming rate. The success of such those international agreements has been very limited until today (Butchart et al., 2019). The Aichi Biodiversity Targets, an adaption of the strategic plan for biodiversity through the Convention on Biological Diversity (CBD) was meant to guide global conservation efforts until 2020 (Convention on Biological Diversity (COP), 2010). However, the progress remained insufficient, as only four out of twenty targets showed good advancement, while global biodiversity kept deteriorating (Butchart et al., 2019). The more recent Kunming-Montreal Global Biodiversity Framework (GBF) has set new goals for 2030 and 2050, underscoring the urgency and scale of action required (Affinito et al., 2025). Achieving these ambitions depends not only on governmental players, it also depends on the commercial sector. Businesses and production systems play a dual role: while they are major drivers of biodiversity loss through land-use conversion and resource extraction, they also possess the financial capacity, technological innovation and operational influence that is needed to contribute meaningfully and sustainably to conservation and restoration efforts (Addison et al., 2020; Stephenson et al., 2022). An effective engagement of private actors is increasingly recognized as essential for meeting global biodiversity goals.

To support both, policy targets and corporate accountability, reliable biodiversity monitoring is critical. Monitoring enables the detection of ecological change and the evaluation of conservation outcomes, and it provides evidence for assessing biodiversity impacts linked to commercial land use (Lindenmayer et al., 2011). While field-based monitoring remains foundational, it is time-consuming, costly, and impractical across large or remote areas (Rhodes et al., 2015). Remote sensing offers a valuable complement, providing large-scale, repeated, and cost-effective observations. With the increasing availability of free satellite

imagery and short revisit intervals, remote sensing has become a promising tool for long-term biodiversity monitoring..

## 1.1 Problem Statement

This work focuses on the region of West Kalimantan in Borneo. Borneo is known to be a global biodiversity (Gaveau et al., 2018). The whole of Indonesia, including Kalimantan, has experienced one of the highest rates of forest loss globally. By 2021, Kalimantan had already lost one-third of its natural forests, mostly due to timber extraction, mining and the fast expansion of industrial agriculture such as oil palm (Leonald and Rowland, 2016). In response, agroforestry systems have been recognized as more sustainable production models. Agroforestry systems can be defined as "A dynamic, ecologically based, natural resource management system that, though the integration of trees on farms and in agricultural landscape, diversifies and sustains smallholder production for increased social, economic, and environmental benefits."(Nair et al., 2021, p. 24). They have multiple positive effects on ecological services opposed to regular agricultural systems like enhanced biodiversity, improved soil fertility, support of microclimate regulation and increased carbon storage (Duffy et al., 2021). Such systems might be increasingly relevant to conservation agendas and private-sector sustainability initiatives. The GBF has its own monitoring framework and highlights thereby the importance of tracking such improvements to support progress towards biodiversity targets and inform future policy (Affinito et al., 2025). However, monitoring agroforestry and reforestation projects remains challenging. Remote sensing provides a potential solution, offering consistent and repeatable observations across large regions. Multiple approaches already used satellite data to estimate biodiversity-related metrics, for example functional diversity metrics and the dynamic habitat index, often derived from spectral indices or by modelling approaches (Hauser et al., 2022; Radeloff et al., 2019).

## 1.2 Research Background

Biodiversity can be described and measured in many ways. One important perspective focuses on functional diversity, which refers to the range and distribution of functional traits within a community (Petchey and Gaston, 2002; Tyagi and Kumar, 2024). Functional traits are plant traits that influence an organism's fitness by "affecting growth, reproduction, and survival within a specific environmental context"(Helfenstein, 2024, p. 203). Looking at their diversity is particularly interesting because they respond directly to environmental conditions. Increased functional diversity is often associated with higher resource-use efficiency and a greater ability to adapt to changing external influences (Schneider et al., 2017).

Satellite remote sensing has increasingly been used to assess functional trait diversity across spatial and temporal scales and in different ecosystems. This is especially beneficial because field-based trait datasets remain limited, particularly in remote areas like the tropics (Jetz et al., 2016). Describing plant traits through spectral indices (e.g.,(Helfenstein et al., 2022)) or modelling approaches (e.g.,(Hauser et al., 2022)) therefore provides a practical and scalable alternative. Despite this potential, it is important to acknowledge that ecosystems each exhibit unique functional and spectral characteristics. Consequently, identifying which traits or trait-describing indices are most suitable for specific ecosystem types remains an active area of research (Zheng et al., 2023). There are three components of functional diversity. Functional richness (FRic) quantifies the volume of trait space occupied by a community, functional evenness (FEve) describes how uniformly species or pixels occupy that trait space, and functional divergence (FDiv) reflects how far data points are distributed from the center of the trait space (Mason et al., 2005). These metrics have already been applied successfully across different ecosystems, elevation gradients, and spatial resolutions ((Hauser et al., 2022; Helfenstein et al., 2022; Zheng et al., 2023).

The study by Hauser et al.(2022) is particularly relevant for this thesis. They evaluated FRic, FDiv, and FEve across a land-use gradient consisting of intact forest, logged forest, and oil-palm plantations. Their results found that intact and logged forests shoed higher functional diversity than oil-palm plantations. One major identified challenge was cloud cover: they selected the single Sentinel-2 image with the lowest cloud cover since mission start and highlighted that mosaicking can mask ecological variation by mixing different acquisition dates. A more recent study by Mederer et al. (2025) further emphasizes the importance of

incorporating temporal dynamics into functional diversity assessments. They found that FRic can vary substantially across seasons, meaning that single-date observations may misrepresent ecosystem functioning. Their study also highlighted the practical challenges posed by the high cloud cover in tropical regions and noted that tropical rainforests often show weak or no seasonality in functional metrics.

Together, these studies show that while remote sensing holds strong potential for functional trait and functional diversity monitoring, key challenges remain. Continuous monitoring approaches are needed, the choice of trait-representing indices must be adapted to ecosystem type, and cloud cover poses a significant constraint, especially in tropical regions.

## 1.3 Study Aim and Research Questions

The aim of this master thesis is to address open questions regarding the potential of satellite remote sensing for long-term monitoring of functional diversity in tropical regions. To investigate this, three contrasting land-cover types agroforestry, natural forest, and oil-palm plantations were selected to represent a gradient of land-use intensity.

The study pursues three main objectives: High cloud cover is a persistent challenge in tropical regions. The first objective is therefore to evaluate how heavy cloud cover can be managed when working with time series, and to assess whether cloud masking can increase the amount of observations to achieve enough temporal coverage for biodiversity-relevant monitoring. The second objective is to identify suitable spectral indices for functional trait description. A set of spectral indices representing different canopy-related functional traits are calculated from Sentinel-2 imagery for the period 2019–2024. These indices are examined for their temporal behavior and for how consistently they differentiate between the three land-cover types. The goal is to evaluate which indices are robust, ecologically interpretable, and potentially suitable for long-term monitoring. Finally, two functional diversity metrics, Functional Richness (FRic) and Functional Divergence (FDiv), are derived from the selected indices. Their values are compared between land-cover types and tracked over time to see whether reforested agroforestry sites follow different trends or responses. Therefore assessing functional diversity across space and time therefore forms the third objective of the study. Based on these identified research gaps and objective, the thesis will address the following research questions:

1. How can high cloud coverage be dealt with when aiming for consistent biodiversity monitoring using satellite remote sensing data?

2. What temporal patterns of functional traits and vegetation indices can be observed within and between areas of different land-cover?

3. How can multiple vegetation indices and functional traits be combined to support effective long-term biodiversity monitoring, and which aspects of biodiversity are feasible to capture with these data?

4. Which of the examined indices or traits are most suitable for continuous biodiversity monitoring given the identified temporal and spatial patterns and the observed sensibility to change and robustness towards external conditions in this use case?

The outcome of this work will contribute to aligning biodiversity monitoring with a practical use case, offering guidance on what has to be kept attention to specifically when approaching functional diversity monitoring possibilities

## 1.4 Collaboration

This thesis was carried out in collaboration with Rahn AG and Forestwise. Forestwise is an agroforestry company operating in West Kalimantan. They reforest formerly degraded forest or former plantation sites and implement agroforestry plots on them. Their main products is illipe nut, but they also encourage the harvest of other forest products. As part of the collaboration, Forestwise provided agroforestry plot boundaries, land-use descriptions, and additional information, which formed the basis for the analysis conducted in this thesis. Additional support was provided by Rahn, a swiss-based chemical company that also specializes in cosmetic raw materials, that partners with Forestwise and co-funds reforestation activities.

# 2 Study Area

The study area of this research is located in the region West Kalimantan, in the Indonesian part of Borneo (see **Figure 1**). Borneo lies on the equator and is surrounded by Malaysia, Indonesia and the Philippines. The island is split into three main regions: Kalimantan, which belongs to Indonesia; Sabah and Sarawak, that both belong to Malaysia; and Brunei, an independent country. West Kalimantan, is one of the largest regions of Borneo. Most of Borneo is characterized by a tropical rainforest climate with a mean annual rainfall of 2901-3500mm in the region of interest and an annual mean temperature of around 27°C. Borneo is influenced by two monsoon systems (Sa'adi et al., 2021). The rainfall-heavy north-east (NE) monsoon, is

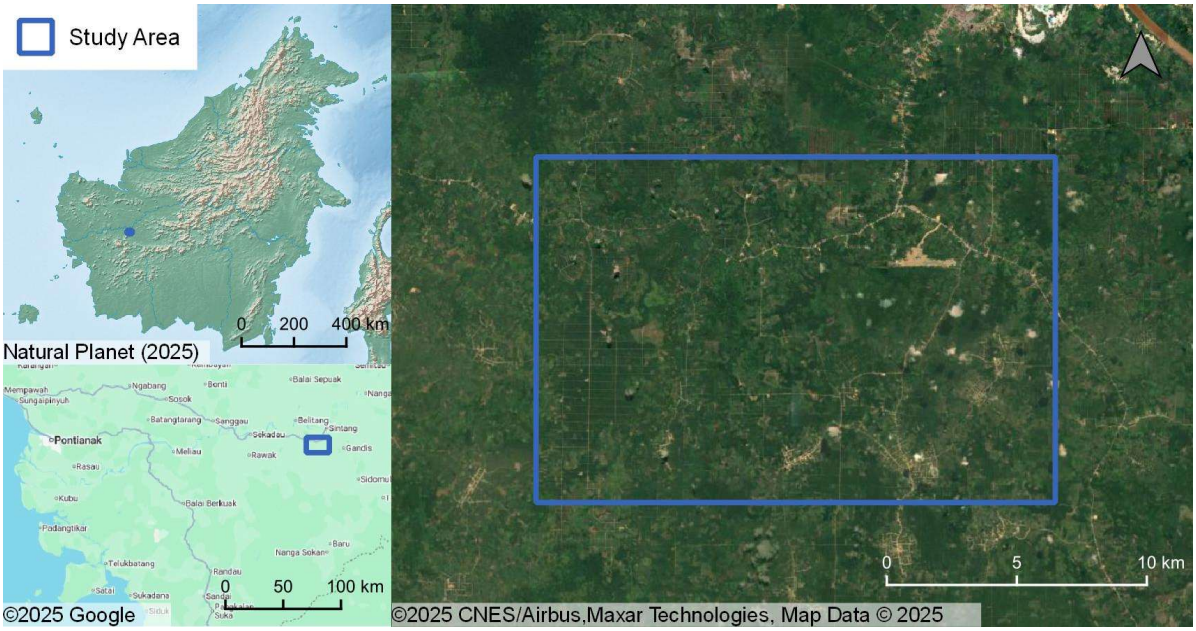


**Figure 1**: Research area in West Kalimantan, Indonesia.

associated with increased precipitation between November and March and the south-west (SW) monsoon from May to September, that brings comparatively dry weather. April and October are considered to be inter-monsoon months and the wettest months are usually from November to February (Sa'adi et al., 2021; Vijith and Dodge-Wan, 2020). According to a West Kalimantan vegetation map by Laumonier et al. (2020), the vegetation in the region of interest is a mosaic of old and young lowland secondary forests, shrubs, agriculturally used areas and long-established as well as newly cleared land for oil palm plantations. These secondary

forests are dominated by lowland tropical forest trees that belong to the family of the Dipterocarpaceae. Primary dipterocarp-dominated forests belong to the most species-rich forests worldwide (Mansur and Brearley, 2023). Unfortunately, Indonesia as a whole has experienced a rapid loss of forested area and Kalimantan is among the most heavily deforested regions of the country. Already about one-third of natural forests have been lost by 2023. The deforestation is mostly driven by mining, agriculture and logging, and in Kalimantan particularly by timber extraction and palm oil production (Mathys et al., 2023). However, secondary forests are also of great importance, as they make up an increasing proportion of the remaining forest cover and play a crucial role in biodiversity conservation and the maintenance of ecosystem services (Mansur and Brearley, 2023).

# 3 Material and Methods

## 3.1 Datasets

This work used a variety of dataset of the analysis. **Table 1** provides an overview of all datasets, including their source and purpose within the analysis. Their respective usage and more detailed information can be found later within the Materials and Methods section.

**Table 1**: Datasets that were used in this work with sources.

| **Dataset** | **Type Description** | **Source** |
|---|---|---|
| Agroforestry Sample Sites: Raw Data | Online Vector Data | Received from Forestwise via (Restor Foundation, 2024) |
| Global Forest Cover map for the year 2020 (GFC) | Forest Cover Map | (Bourgoin et al., 2024) |
| High-resolution global map of smallholder and industrial closed-canopy palm plantations 2019 | Palm Plantation Map | (Descals et al., 2021a) |
| PlanetScope Imagery | Remote Sensing Data | (Planet Labs PBC, 2025) |
| Harmonized Sentinel-2 MSI Collection: MultiSpectral Instrument, Level-2A (SR) (Sen2_Harmonized). | Remote Sensing Data | (European Space Agency, 2022) |
| Cloud Score+ S2_HARMONIZED V1 (CS+) | Remote Sensing Data | (Pasquarella et al., 2023) |

## 3.2 Software and Packages

The following analysis was conducted using Python for the whole processing pipeline and QGIS for data preprocessing and similar work. To access and process remote sensing data the python API of Google Earth Engine (GEE) was used. **Table 2** summarizes all software tools and Python packages used in this study, including version numbers and sources.

**Table 2**: Software and python packages that were used in this work with sources.

| **Software/Package** | **Version** | **Purpose** | **Source** |
|---|---|---|---|
| QGIS | 3.16.11 | Preprocessing, data preparation | (QGIS Development Team, 2025) |
| Jupyter Notebook | 7.3.2 | Coding environment | - |
| Python | 3.12.9 | Core environment | - |
| pandas | 2.2.3 | Data handling and table operations | (The pandas development team, 2024) |
| geopandas | 1.0.1 | Geodata handling | (Van den Bossche et al., 2024) |
| shapely | 2.1.2 | Geodata handling | (Gillies et al., 2025) |
| numpy | 2.2.3 | Data handling and numerical operations | (Harris et al., 2020) |
| earthengine-api | 1.5.2 | Cloud-based remote sensing imagery processing | (Gorelick et al., 2017) |
| geemap | 0.35.1 | Converting local geometry to cloud geometry | (Wu, 2020) |
| scipy | 1.15.2 | Convex hull calculation and statistics | (Virtanen et al., 2020) |
| seaborn | 0.13.2 | Plotting | (Waskom, 2021) |
| maplotlib | 3.10.0 | Plotting | (The Matplotlib Development Team, 2024) |

## 3.3 Preprocessing

### 3.3.1 Agroforestry Sample Sites

The agroforestry sample sites were obtained from the website 'restore.eco' where they had been uploaded by Forestwise: The sample sites include areas where Forestwise, in partnership with Rahn, began reforesting in October or November 2022. Before reforestation, the plots featured different types of vegetation, including some that had been plantations until shortly before. The reforestation approach primarily involved planting illipe trees of about 1 year of age.

These polygons were then drawn off by manually in QGIS with the help of PlanetScope orthophotos, to ensure accurate spatial placement. This initial dataset had a total of 24 sample sites. Following the digitization of those sample sites from the website, they were preprocessed to correct spatial misalignments and improve accuracy. as the initial polygons appeared shifted, some too small for the intended analysis, and inconsistent when compared to georeferenced orthophotos as, for example they strongly overlapped with nearby infrastructure

First four polygons with a size of less than 0.5 ha were excluded from the analysis. Helfenstein (2024) found that diversity patterns below 1 ha or even 1.1 ha are not detectable anymore when working with Sentinel-2 data at 20m resolution. As 15 sample sites were smaller than 1 ha, applying a buffer to the polygons was necessary. However, expanding them beyond twice their original size was deemed unreliable. Therefore, polygons smaller than 0.5 ha were excluded from the analysis.

In a second step the sample sites were compared to the PlanetScope images with a frequency of one image every half a year. Several sample sites appeared to be bare for extended periods of time or contained areas of other land covers (e.g., roads). After the examination of these images, four additional sites were deemed unsuitable and excluded from the analysis, resulting in a final set of 16 sample sites.

In the third step, some polygons required spatial adjustment as they exhibited misalignment when compared to orthophotos and overlapped with adjacent infrastructure (see **Figure 2a**). Finally, the remaining sites were incrementally buffered to reach a

standardized size of 1.1 ha (see **Figure 2b**). This procedure yielded the definitive set of agroforestry sample sites for the study (see **Figure 3**).

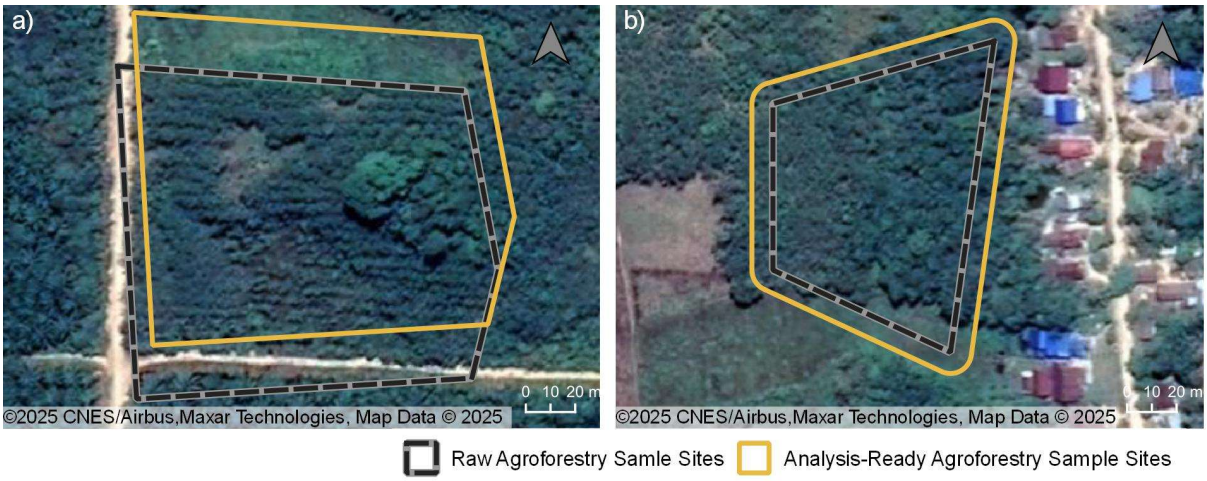


**Figure 2**: Examples of how the initial agroforestry sample sites were preprocessed. Image a) shows a sample site that was shifted to prevent overlaps with the nearby road. Example b) shows a site that had to be buffered in order to reach the required 1.1 ha

### 3.3.2 Natural Forest and Palm Plantation Sample Sites

The sample sites for the land cover categories 'Natural Forest' and 'Palm Plantation' were acquired with the help of PlanetScope data, accessed via QGIS, and two supplementary datasets estimating the extents of the corresponding land cover type. This approach including several sources ensured improved reliability and consistency in spatial representation across all analyzed years by integrating PlanetScope orthophotos with complementary land cover datasets. The digitization of the natural forest sample sites was based on the European Union's work titled "Mapping Global Forest Cover of the Year 2020 to Support the EU Regulation on Deforestation-free Supply Chains", which produced the "Global Forest Cover map for the year 2020" (GFC2020) at a 10m resolution (European Commission. Joint Research Centre. et al., 2024). They define 'forest' by the definition of the Food and Agriculture Organization (FAO), that is:

> "Land sparring more than 0.5 hectares with trees higher than 5 meters and a canopy cover of more than 10 percent, or trees able to reach these thresholds in situ. It does

not include land that is predominantly under agricultural or urban land use."(Food and Agriculture Organization, 2018, p. 4)

The definition also explicitly mentions that trees in agricultural production system, like oil-palm plantations are not part of this definition for forest. In this work, it shall be added that the land cover category 'Natural Forest', also called 'Forest' sometimes for better readability, will refer to unmanaged forests, that are also not part of agroforestry systems. The GFC2020 dataset builds on several global datasets, mostly based on remotely sensed data. Those are analyzed and merged to retrieve the 2020 forest layer that was used here.

The digitization of the palm plantation followed a dataset produced by Descals et al. (2021a), which is a product of their study 'High-resolution global map of smallholder and industrial closed-canopy palm plantations' (Descals et al., 2021b). They defined oil-palm plantations mostly by their structure:

"An industrial oil palm plantation typically covers several thousand hectares of land and is very well structured and homogeneous in tree age. It consists of an area bounded by long linear, sometimes rectangular boundaries. (…)"(Descals et al., 2021b, p. 1215)

The global map of closed-canopy oil palm plantations represents the year 2019, has a spatial resolution of 10 m and was generated using a convolutional neural network that classified Sentinel-1 and Sentinel-2 imagery.

The dataset resulting from all preprocessing steps consist of a set of 46 polygons. The statistics are in **Table 3** and the full set of sample sites is visible in **Figure 3**. A map where one can see the structure of each of the three land-cover sites in an example can be seen in the appendix in **Figure A. 1**.

**Table 3:** Sample Site Dataset, with sample size (n), area and median elevation in m above sea level (a.s.l.) of each land cover type.

| Land cover Type | n | Total Area (ha) | Median Elevation (m a.s.l.) |
|---|---|---|---|
| Forest | 15 | 19.6 | 29.1 |
| Agroforestry | 15 | 20.3 | 28.2 |
| Palm Plantation | 16 | 20.0 | 33.5 |

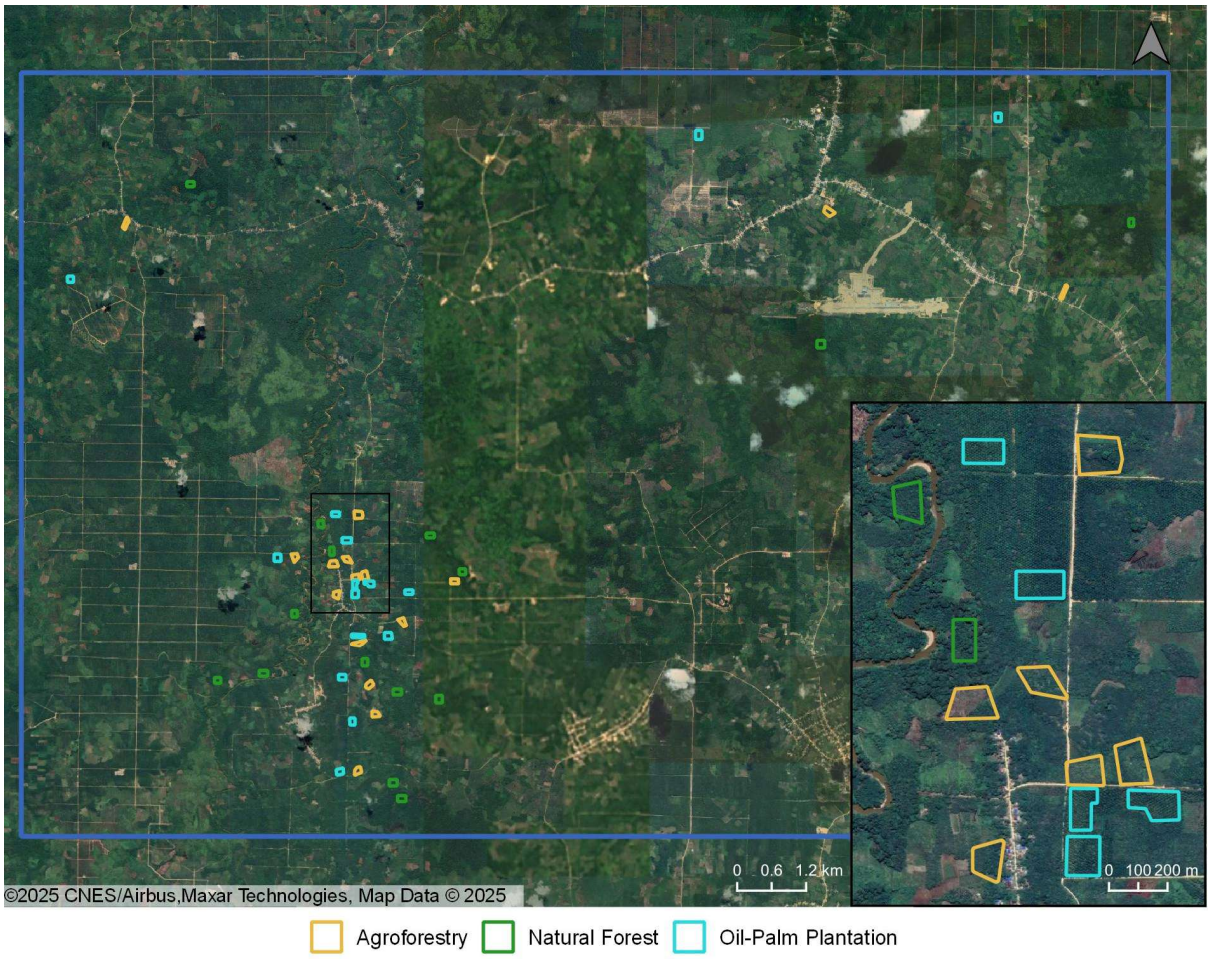


**Figure 3**: Overview over the whole sample site dataset after preprocessing. Most of the sites are clustered on the southern part of the study area. The small window on the right hand side of the map offers a closer view to some of the sample sites.

### 3.3.3 Satellite Remote Sensing Data

The following analysis will use images from the European Space Agencies (ESA) Sentinel-2 mission, which is part of the Copernicus Program and offers high-resolution, multi-spectral imagery with a revisit time of 5 days at the equators (Korhonen et al., 2017b). The mission currently consists of three satellites (Sentinel-2A, Sentinel-2B and Sentinel-2C), whereof only Sentinel-2A and Sentinel-2B are relevant for this analysis. Each satellite carries an optical Multi-Spectral Instrument (MSI) that samples 13 spectral bands at different spatial and spectral resolutions (see **Table 4**) (Korhonen et al., 2017a).

**Table 4**: Sentinel-2A MSIs spectral bands and their spatial and spectral resolution (Korhonen et al., 2017, p. 260)

| Band | Band Name | Central Wavelength (nm) | Bandwidth (nm) | Spatial Resolution (m) |
|---|---|---|---|---|
| B1 | Coastal aerosol | 442.7 | 21 | 60 |
| B2 | Blue | 492.4 | 15 | 10 |
| B3 | Green | 559.8 | 36 | 10 |
| B4 | Red | 664.6 | 31 | 10 |
| B5 | Vegetation red-edge 1 | 704.1 | 15 | 20 |
| B6 | Vegetation red-edge 2 | 740.5 | 15 | 20 |
| B7 | Vegetation red-edge 3 | 782.8 | 20 | 20 |
| B8 | Near Infrared (NIR) | 832.8 | 106 | 10 |
| B8A | Narrow NIR | 864.7 | 21 | 20 |
| B9 | Water vapor | 945.1 | 20 | 60 |
| B10 | SWIR-Cirrus | 1373.5 | 31 | 60 |
| B11 | SWIR 1 | 1613.7 | 91 | 20 |
| B12 | SWIR 2 | 2202.4 | 175 | 20 |

The data was accessed via GEEs Sentinel-2 Harmonized collection (Sen2_Harmonized). The Sentinel-2 Harmonized collection offers analysis-ready Level-2A surface reflectance products that integrates imagery from Sentinel-2A and Sentinel-2B. The data is atmospherically,

radiometrically and geometrically corrected, using the “Sen2Cor” Algorithm (European Space Agency, 2022).

### 3.3.4 Cloud Masking

Removing cloud or cloud-shadow covered pixel from the images before the analysis is crucial for receiving clear and reliable observations. A common method for cloud masking in GEE is the use of the dataset "Cloud Score+ S2_HARMONIZED V1" (CS+) (Pasquarella et al., 2023). CS + is derived from Sentinel-2 Level 1C data and provides a per-pixel probability score indicating the extent to which pixels are affected by clouds or cloud shadows. This score is generated using a machine learning model that considers factors such as image brightness and texture (Le Minh Hang et al., 2024). Le Minh Hang et al. (2024) evaluated several cloud masking methods using Sentinel-2 data and determined that applying a threshold of 0.6 on the cs-band of Cloud Score+ resulted in an accuracy of 91.5%, ranking it among the most effective cloud masking approaches (Le Minh Hang et al., 2024). Given that their study was conducted in a comparable setting, a lowland forest with high humidity and an average annual temperature of 25°C, the threshold was adopted for the present work.

### 3.3.5 Vegetation Mask

One of the most common indices used for vegetation mapping in remote sensing is the normalized difference vegetation index (NDVI). The NDVI works by the principle that vegetation has a high reflectance in the near infrared wavelength region and a low reflectance in the visible red wavelength region, making use of the contrast between these channels in vegetation (Wani et al., 2021). The NDVI will be used for vegetation masking by thresholding. To determine an appropriate threshold value the Otsu algorithm was used (Otsu, 1979). The Otsu algorithm is an automatic thresholding method that separates values into two distinct groups by testing every possible threshold value on its ability to generate groups, using the histogram. The algorithm is frequently used for image binarization (Otsu, 1979). The image processing in this step was carried out in a Jupyter notebook, with python and using the GEE API.

The following steps were done iteratively for each year within the targeted time period. Only the agroforestry land cover type was considered, as the other land cover types were

intentionally drawn to avoid crossing non-vegetated areas. The Sen2_Harmonized image collection was first filtered spatially by the respective site boundaries and by the target year. The remaining images were then extended by adding an NDVI band and the CS+ band. Then, the median pixel values across all images of the respective year were calculated. These median pixel values were transformed into a histogram, which served as the basis of the Otsu algorithm. The Otsu algorithm proceeds as follows: First, the pixel count in each histogram bin is normalized by the total number of pixels, resulting in a probability value per bin. The cumulative sum of these probabilities is then computed, showing the likelihood of a pixel falling into a bin up to that target bin. Next, the cumulative average NDVI value for each bin is calculated by weighting bin values with their probabilities. Using these values and the overall mean NDVI, the algorithm computes the interclass variance for every possible bin, comparing two groups formed by the threshold (the central NDVI value of that bin). The bin with the highest interclass variance is selected as the optimal threshold (Otsu, 1979).

From these yearly thresholds, the lowest value was chosen, NDVI=0.58 in 2020, for the reason that some of the agroforestry sample sites are still in the process of reforestation. A threshold values that is too high might exclude too much of that vegetation from the analysis. Also, the natural forest and oil-palm plantation sample sites were drawn specifically to not include other land cover. The corresponding histogram is shown in **Figure 4**.

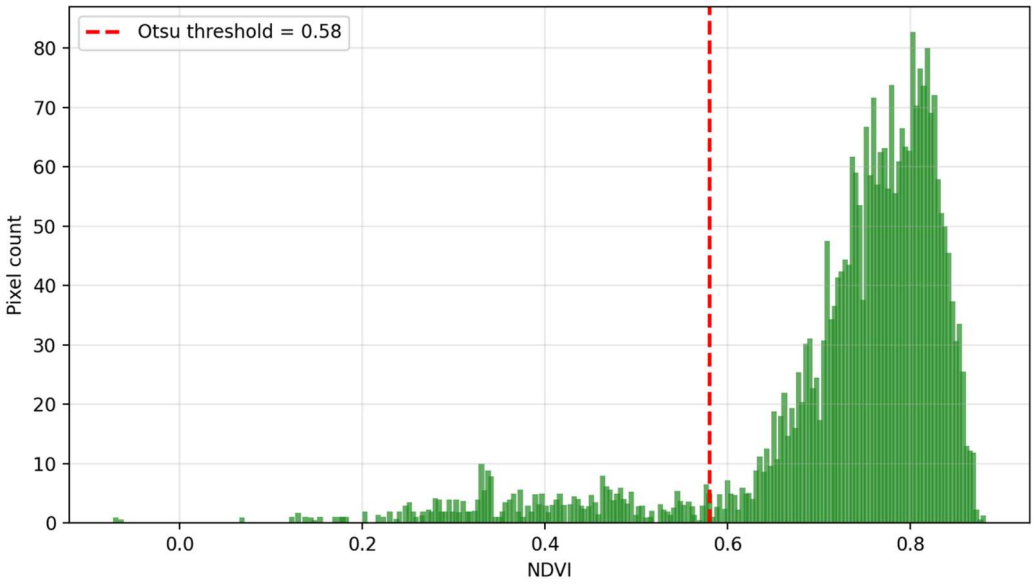


**Figure 4** : Histogram of all mean NDVI values per pixel of the agroforestry sample plots in 2020. The red line indicates the threshold determined by the Otsu calculation at 0.58.

## 3.4 Spectral Indices as Approximation for Canopy Functional Traits

Plant traits can be grouped into several classes and types, such as morphological traits (e.g., leaf area) or physiological traits (e.g., chlorophyll content or leaf water content) or phenological traits (e.g., leaf senescence) among others (Rao et al., 2024). For satellite remote sensing canopy functional traits are the most relevant because they are visible to the spectral sensors. Besides canopy traits are important, as they form the main interface between forest and atmosphere and therefore are related closely to processes like transpiration or photosynthesis (Aguirre-Gutiérrez et al., 2025).

The following section presents the spectral indices selected to describe canopy functional traits and provides an overview of their use in the scientific literature.

### 3.4.1 General Vegetation Indices

**Table 5**: List of general vegetation indices that will be used in this analysis.

| **Index Name** | **Original Sources** | **Formula** |
|---|---|---|
| Normalized Difference Vegetation Index (NDVI) | (Kriegler, 1969) | (Zhao et al., 2020) |
| Optimized Soil-Adjusted Vegetation index (OSAVI) | (Rondeaux et al., 1996) | (Zhao et al., 2020) |
| Enhanced Vegetation Index (EVI) | (Huete et al., 2002) | (Son et al., 2020) |

The analysis will include some general vegetation indices, from now on called 'greenness' describing indices, to compare to the other trait describing indices, and the help to check if they are plausible. The used indices are summarized in **Table 5**. The NDVI, that was used for masking will be calculated, then the Optimized Soil Adjusted Vegetation Index (OSAVI), an alternative to the NDVI that intends to mitigate effects of soil that could introduce bias and also the Enhanced Vegetation Index (EVI). that is less prone to saturation in temperate and tropical forests.

$$NDVI = \frac{R_{842} - R_{665}}{R_{842} + R_{665}} \tag{3-1}$$

$$OSAVI = (1 + 0.16) \times \frac{R_{783} - R_{665}}{R_{783} + R_{665} + 0.16} \quad (3\text{-}2)$$

$$EVI = 2.5 \times \frac{R_{842} - R_{665}}{R_{842} + (6 \times R_{665}) - (7.5 \times R_{490}) + 1} \quad (3\text{-}3)$$

### 3.4.2 Chlorophyll Content

Chlorophyll is a green pigment and photoreceptor, usually sitting in the leaves chloroplasts (Mielke et al., 2012). It is responsible for primary photosynthesis in plants, captures incoming light and is therefore a driver for carbon fixation. The amount of chlorophyll in vegetation is tightly related to important ecological variables and plant functional traits, like the photosynthetic capacity or primary productivity. Like with most pigments, variations in the amount of chlorophyll can give indications on overall plant health and on possible environmental stressors like drought, changes in nutrient availability, temperatures out of the normal range or other disturbances (Talebzadeh and Valeo, 2022). The distinctive reflectance spectrum of chlorophyll, renders it suitable for an analysis via spectral reflectance. This is also reflected by the extensive variety of existing spectral indices to estimate chlorophyll content. Chlorophyll absorbs light particularly in the blue and red region of the visible spectrum and has low light absorption in the NIR region (750-900nm). Other interesting features of the absorption spectrum are the so-called red- and green-edge regions: The red-edge region (~700nm) is mainly caused by chlorophyll-a and is characterized by a rapid change from high to low absorption and therefore very sensitive to changes in chlorophyll concentration. The green-edge region (~500-550nm) is close to an inflection point of the absorption spectrum as well, but influenced by both chlorophyll-a and chlorophyll-b, as well as by carotenoids (Kior et al., 2021). Huang et al. (2015) conducted a meta-analysis of 85 different studies to examine the predictive relationship between spectral data and chlorophyll concentration. The literature covered a variety of scales (leaf, canopy and landscape) and vegetations types. The analysis revealed that while chlorophyll-a, chlorophyll-b and total-chlorophyll could be reliably predicted at the level of individual leaves, predictions at the canopy level were only valid for total chlorophyll estimations. The authors recommend the use of wavelengths in the green (550-560nm) or the red-edge (680-750nm) region to estimate total chlorophyll content at

canopy level (Huang et al., 2015). Additionally, Cui et al. (2019) discovered that the estimation of leaf chlorophyll content estimation in wheat with Sentinel-2 is improved when longer wavelengths of the red-edge bands are employed.

There is a large variety of indices that aim to estimate chlorophyll content. The following table contains the chlorophyll describing indices tested in this work.

**Table 6:** Indices considered for chlorophyll estimation with sources.

| **Index Name** | **Original Sources** | **Formula** |
|---|---|---|
| Red-edge Chlorophyll Index ($Cl_{red-edge}$) | (Clevers and Gitelson, 2013) | (Clevers and Gitelson, 2013) |
| Green Chlorophyll Index ($Cl_{green}$) | (Clevers and Gitelson, 2013) | (Clevers and Gitelson, 2013) |
| TCARI/OSAVI | (Haboudane et al., 2002) | (Clevers and Gitelson, 2013) |
| MERIS Terrestrial Chlorophyll Index (MTCI) | (Dash and Curran, 2004) | (Clevers and Gitelson, 2013) |
| Normalized Difference Red-Edge 1 (NDRE1) | (Gitelson and Merzlyak, 1994) | (Padalia et al., 2020) |
| Normalized Difference Red-Edge 2 (NDRE2) | (Barnes, E. M. et al., 2000) | (Clevers and Gitelson, 2013) |
| Simple Ration ($SR_{R740/R705}$) | (Padalia et al., 2020) | (Padalia et al., 2020) |

The chlorophyll index red edge ($Cl_{red-edge}$) and the green chlorophyll index ($Cl_{green}$) were both defined in Clevers and Gitelson (2013) and initially used for the estimation of chlorophyll in grass and crops.

$$CI_{red-edge} = \left(\frac{R_{783}}{R_{705}}\right) - 1 \tag{3-4}$$

$$CI_{green} = \left(\frac{R_{783}}{R_{560}}\right) - 1 \tag{3-5}$$

Both indices have the advantage of avoiding the saturation effect observed in traditional greenness indices such as the NDVI. $Cl_{red\text{-}edge}$ uses the red-edge position and has been applied in a variety of scenarios, showing promising accuracy for the use in tropical settings on leaf and canopy levels (Mielke et al., 2012; Padalia et al., 2020). On the other hand, there seems to be limited research on the use of the $Cl_{green}$ index for tropical settings. Zarco-Tajada et al. (2019) found that it has the most linear relationship to the chlorophyll concentration in a Mediterranean conifer forest, compared to indices relying more on red-edge regions.

Three other frequently used indices are the modified chlorophyll absorption ratio index (MCARI) by Daughtry et al. (2000) and the transformed chlorophyll absorption ratio index (TCARI) by Haboudane et al. (2002). Both TCARI and MCARI rely on the same bands (if applied with Sentinel-2), but MCARI is influenced more by LAI, low chlorophyll and background reflectance. TCARI mitigates effects of nongreen biomass effects but is still sensitive to background reflectance. The ratio of TCARI/OSAVI was then introduced to retrieve accurate predictions of crop chlorophyll (Haboudane et al., 2002), by trying to minimize the effect of background reflectance on chlorophyll description. While the ratio TCARI/OSAVI was initially validated with crop data, Ferreira et al. (2018) compared the index to estimates derived from a 3D radiative transfer model. The results suggested that the index is valid for tropical settings, even though initially not developed for it (Ferreira et al., 2018). In this work a multispectral adaptation seen in Wang et al. (2022) will be used.

$$\frac{TCARI}{OSAVI} = 3 * \frac{\left((R_{740} - R_{705}) - 0.2 * (R_{740} - R_{560}) * (R_{740} - R_{705})\right)}{\left((1 + 0.16) * \left(\frac{R_{740} - R_{705}}{R_{740} + R_{705} + 0.16}\right)\right)} \quad (3\text{-}6)$$

The 'MERIS Terrestrial Chlorophyll Index' (MTCI) has originally been developed for the Medium Resolution Imaging Spectrometer (MERIS) sensor, but can also be calculated using Sentinel-2, due to similar placement of their red-edge bands (Clevers and Gitelson, 2013). Studies have found that the MTCI performs well at estimating canopy chlorophyll content in agricultural settings (Clevers and Gitelson, 2013). Dash (2010) used MTCI (applied with METS) for a phenological analysis of Indian ecosystems, and found that METIS is a reliable tool for monitoring (chlorophyll-based) phenology in seasonal, tropical rainforests.

$$MTCI = \frac{R_{740} - R_{705}}{R_{705} - R_{665}} \quad (3\text{-}7)$$

Two other widely applied chlorophyll estimation indices are the Normalized Difference Red Edge Indices NDRE1 and NDRE2. Gitelson and Merzlyak (1994) originally proposed NDRE1 as an index to estimate leaf level chlorophyll in chestnut and maple. NDRE2 was introduced in Barnes (2000) to asses canopy chlorophyll of cotton crops. The difference between NDRE1 and NDRE2 is that NDRE2 generally uses red-edge bands, while NDRE1 relies on one red-edge and one NIR band. NDRE1 seems to be used more often than NDRE2 and has shown promising results in estimating canopy chlorophyll contents in various contexts. Kanu et al. (2025) found a linear relation between satellite-derived NDRE1 values and leaf chlorophyll content in a tropical partially evergreen forest in the Himalaya region. Similarly, Padalia et al. (2020) has identified NDRE1 as one of the most successful canopy chlorophyll estimators for tropical forest plantation in the sub-tropical part of North India.

$$NDRE1 = \frac{R_{740} - R_{705}}{R_{740} + R_{705}} \quad (3\text{-}8)$$

$$NDRE2 = \frac{R_{783} - R_{705}}{R_{783} + R_{705}} \quad (3\text{-}9)$$

Padalia et al. (2020) also found a simple ratio among the most successful estimators, which was therefore included in this work as well.

$$SR_{740/705} = \frac{R_{740}}{R_{705}} \quad (3\text{-}10)$$

### 3.4.3 Water Content

Vegetation water content describes the amount of water in vegetation relative to its dry matter (Ievinsh, 2023). Water content of crops and agricultural vegetation has particularly been a primary focus, due to its importance in decision-making processes related to controlled irrigation and drought mitigation strategies (Cheng et al., 2008; Mirzaie et al., 2014; Wang et al., 2009).

Within the absorption spectrum of vegetation, the most important regions for estimating water content lie in the near- and shortwave-infrared wavelengths. More specifically, strong absorption features occur at 750-900nm, 1200nm, 1450nm and 1940nm (Kior et al., 2021). However, Sims & Gamon (2003) found that bands around 1450nm and 1940nm are not ideal for optical remote sensing applications, as solar irradiance is low at these wavelengths and atmospheric water vapor might interfere with reflected signals. They also mentioned that the 950-970nm region may be compromised by atmospheric vapor. Instead, they recommended the use of wavelengths around 1150-1260nm or 1520-1540nm.

**Table 7:** Indices used for canopy water estimation with sources.

| **Index Name** | **Original Sources** | **Formula** |
|---|---|---|
| Normalized Difference Water Index (NDWI) | (Gao, 1996) | (Helfenstein, 2024) |
| Normalized Difference Infrared Index (NDII) | (Hardisky et al., 1983) | (Zhou et al., 2022) |
| Moisture Stress Index (MSI) | (Hunt and Rock, 1989) | (Dotzler et al., 2015) |
| Normalized Multi-Band Drought Index (NMDI) | (Wang and Qu, 2007) | (Cavalaris et al., 2021) |

Research that tries to validate vegetation canopy water indices seem to focus mostly on agricultural use cases. Most of the studies target sparse vegetation or crops (Colombo et al., 2008; Varghese et al., 2021; Yilmaz et al., 2008). Nevertheless, most of the indices applied here have been used in tropical settings. A frequently used index is the Normalized Difference Water Index (NDWI). The index was introduced by Gao (1996) and has since then proven its usability in various contexts, also in tropical settings, for example to monitor drought patterns in seasonally dry tropical forests (Ferreira et al., 2024). While the original index uses a spectral band at 1240 nm (a wavelength that is not available from Sentinel-2 data), studies have replaced this band with the band at 1610 nm, what makes the index extremely similar to the Normalized Difference Infrared Index (NDII) (Gao, 1996; Helfenstein, 2024).

$$NDWI = \frac{R_{842} - R_{1610}}{R_{842} + R_{1610}} \quad (3\text{-}11)$$

Yilmaz et al. (2008) found the NDII to be linearly related to canopy water content in a variety of vegetation types, which is supported by the findings from Zhou et al. (2022).

$$NDII = \frac{R_{865} - R_{1610}}{R_{865} + R_{1610}} \quad (3\text{-}12)$$

The Moisture Stress Index (MSI) is another frequently applied index that has a linear relationship with vegetation water stress, thus exhibiting a negative linear relationship with vegetation water content (Colombo et al., 2008). In this work the inverted version will be used, such that the correlation with more canopy water is positive (Dotzler et al., 2015; Helfenstein, 2024).

$$MSI = \frac{R_{842}}{R_{1610}} \quad (3\text{-}13)$$

The Normalized Difference Multi-Band Drought Index was initially proposed by Wang and Qu (2007) to monitor soil and vegetation moisture. The index is only applicable for either bare soil or heavily vegetated areas (Leaf Area Index(LAI) greater than 2), as otherwise soil and vegetation moisture conditions mix and cannot be interpreted accurately. Otherwise, the index is similar to the NDWI and the NDII, where lower index values indicate less moisture. The NMDI has been primarily used as an indicator for evaluating fire risk, demonstrating effective performance in tropical settings (Oliveira Santos et al., 2021).

$$NMDI = \frac{R_{842} - (R_{1610} - R_{2190})}{R_{842} + (R_{1610} - R_{2190})} \quad (3\text{-}14)$$

### 3.4.4 Other Pigments

Anthocyanins and carotenoids are two of the most important plant pigments besides chlorophyll (Zhao et al., 2022). Carotenoids play an important role in photosynthesis, by being able to absorb additional light, especially at the blue-green wavelength regions that aren't well

absorbed by chlorophyll (Hashimoto et al., 2016; Mielke et al., 2012). The yellow, orange or red pigment also protects leaves from damage by solar radiation by passing excess energy to the xanthophyll cycle, from where it is released as heat (Nunes et al., 2019). Similar to Carotenoids, Anthocyanins' most important function is their role as photoprotector in foliage. The plant pigment, which usually gives red, blueish or violet hues to plants, is produced mostly in response to stressors like drought or low temperature stress or during the stage of early leaf development (Li and Ahammed, 2023; Papes et al., 2013). Anthocyanins show an absorption peak at around 550nm (Papes et al., 2013).

**Table 8**: Indices considered for pigment description with sources.

| **Index Name** | **Original Sources** | **Formula** |
|---|---|---|
| Anthocyanin Reflectance Index (ARI1) | (Gitelson et al., 2001) | (Helfenstein, 2024) |
| Modified Anthocyanin Reflectance Index (mARI) | (Gitelson et al., 2006) | (Helfenstein, 2024) |
| Carotenoid Reflectance Index 550 ($CRI_{550}$) | (Gitelson et al., 2007) | (Montes-Bojórquez et al., 2025) |
| Plant Senescence Reflectance Index (PSRI) | (Merzlyak et al., 1999) | (Cohen et al., 2024) |

Two known indices for anthocyanin estimation are the Anthocyanin Reflectance Index 1 and the Modified Anthocyanin Reflectance Index (mARI) (Gitelson et al., 2006, 2001). Both indices were used in several studies, for agricultural settings or for monitoring of forest health (Bayle et al., 2019; Bayona et al., 2018; Gupta and Pandey, 2021; Lee et al., 2023). Gitelson et al. (2006) tested mARI on dogwood and maple, and found the index to account for 93% of anthocyanin variation. The paper mentions that the choice of wavelength may have to be adjusted to the respective species. No paper was found that validates either of the indices for a setting as the one in this work. The modified version of ARI1 was proposed to minimize the

impact of leaf thickness and density, but Bayle et al. (2019) found that there is no real difference between the two indices.

$$ARI1 = \frac{1}{R_{560}} - \frac{1}{R_{705}} \tag{3-15}$$

$$mARI = R_{783}\left(\frac{1}{R_{560}} - \frac{1}{R_{705}}\right) \tag{3-16}$$

The Carotenoid Reflectance Index (CRI1) was introduced by Gitelson et al. (2007), on the example of maple, chestnut and beech. The authors found that, just as chlorophyll, the carotenoid content was closely related to reflectance at around 550nm. To remove the effect of chlorophyll, a band between at either 550 nm or 700 nm has to be used, which is proportional to the chlorophyll content (Gitelson et al., 2007). Montes-Bojórquez et al. (2025) tested several configurations of the CRI1, by comparing it to simulated data across a variety of landscapes. Therefore, this work will use CRI1 with the band at 560nm, that performed best in their study, especially under conditions with a high LAI .

$$CRI1 = \frac{1}{R_{490}} - \frac{1}{R_{560}} \tag{3-17}$$

The Plant Senescence Reflectance Index (PSRI) was introduced by Merzlyak et al. (1999) and is sensitive to the carotenoid/chlorophyl ratio. It can be used as a quantitative measure of leaf senescence, where higher values typically indicate higher stress level or more aging vegetation (Merzlyak et al., 1999). While research on the accuracy of PSRI in tropical environments seems limited, the index has successfully been used to monitor the rehabilitation processes of degraded forests in the Mediterranean and Türkiye (Çinar et al., 2025; Cohen et al., 2024).

$$PSRI = \frac{R_{665} - R_{490}}{R_{740}} \tag{3-18}$$

### 3.4.5 Leaf Area Index

The LAI is a measurement describing how much leaf surface interacts with light. It describes the total one-sided leaf area per unit ground area and is essential for primary productivity, influences a canopies water household and therefore biochemical and ecological functioning. Calculating the LAI from multispectral sensory like Sentinel-2 is mostly done with physical models, as empirical approaches such as indices are region specific or tend to have a saturation problem. Pasqualotto et al. (2019) introduced the Sentinel-2 LAI Index (SeLI), which was tested with a variety of different crop types and seems stable up to an LAI of 5.

$$SeLI = \frac{R_{865} - R_{705}}{R_{865} + R_{705}} \tag{3-19}$$

### 3.4.6 Functional Diversity Metrics

In this study, FRic and FDiv were calculated as seen in Helfenstein et al. (2022). As described in the introduction, FRic represents the volume of the convex hull that encloses all pixels in a trait space. Higher FRic values indicate that a community or sample site occupies a larger portion of trait space, suggesting a greater range of ecological strategies or functions (Schneider et al., 2017). FRic was calculated here using the ConvexHull function from the SciPy package. Functional divergence (FDiv), in contrast, reflects how trait values (or in this case, index values) are distributed relative to the center of gravity of the trait space. High FDiv values indicate that trait values cluster toward the edges of the occupied trait space, suggesting greater niche differentiation, whereas low values indicate clustering near the center. FDiv was calculated as the mean distance of all pixels to the center of gravity of the trait space (Schneider et al., 2017).

## 3.5 Data Processing

### 3.5.1 Observation Frequency

Determining the frequency for computing indices is essential. For reforestation monitoring, tracking only a few times per year may be enough. However, seasonality can affect results. Therefore, the choice was made to use one image per month. To select the best image each month, images were filtered by a cloud score threshold median of 0.6 and only images with a median CS+ above this threshold were kept. From the remaining images, the one with the smallest CS+ median was chosen. Similar approaches have been employed in other studies focused on forest monitoring (Van Passel et al., 2020).

### 3.5.2 Processing Pipeline for Index Calculation

A processing pipeline was established. The pipeline iterates over each sample site polygon, and within each polygon, processes every year and month specified for analysis. The Sen2_Harmonized image collection is filtered by year and month, then enhanced by adding NDVI and CS+ bands. Images with a polygon-level median CS+ value below 0.6 are excluded to ensure data quality. The filtered collection is sorted by median CS+, to then select the image with the lowest cloud cover for further processing. This selected image is clipped to the polygon boundaries and calibrated by scaling digital number (DN) values to reflectance by division through 10,000. All spectral indices are calculated at the spatial resolution corresponding to the coarsest band involved (NDVI, EVI, CRI1 at 10m, the rest at 20m). At last, the mean index values per polygon are extracted and stored in a table, alongside essential metadata such as the count of masked pixels and image identifiers.. This table then served as a base for generating plots and statistically evaluating the results. A schematic representation of the pipeline is depicted in Appendix (see **Figure A. 2**).

### 3.5.3 Processing Pipeline for Retrieving Functional Diversity Metrics

Images resulting from the steps in section 3.5.2 were processed further to retrieve the functional diversity metrics. For three selected spectral indices, all scenes were iterated over and every pixel value was extracted from the respective band in order to obtain global

minimum and maximum values for each index. These per-index minimum and maximum values were then used to normalize each band to a range between 0 and 1 (Hauser et al., 2022).

Outlier removal was necessary before computing the metrics as especially FRic is very sensitive to outliers (Helfenstein, 2024). Removing a fixed percentage of values per sample site was not practical, as many sites are only 1.1 ha in size, what is the minimum needed for functional diversity calculations and this would have led to a high loss of scenes therefore. The Mahalanobis distance was applied as a statistical outlier detection method (McLachlan, 1999). It assumes normal distribution of datapoints, calculates the values for 5% quantile outliers (two-tailed) and removes datapoints of that value if present in the pixel set. This method is not ideal since the pixel values are probably not normally distributed. However, comparing the results to the same results calculated without outlier removal indicates that the method seems to at least reduce some extreme values.

After this step both functional diversity metrics were calculated. The results were extracted and saved to a table. The pipeline is depicted schematically in the Appendix (**Figure A. 2**).

### 3.5.4 Statistical Evaluation

The retrieved results were statistically evaluated. For relations between categorical and numerical variables (e.g., land cover type and index values) the Kruskal-Wallis test was used, as conditions for an ANOVA weren't met. For correlations the Pearson correlation was used. Both, the Pearson correlation and the Kruskal-Wallis test were calculated with the SciPy python package (Virtanen et al., 2020).

# 4 Results

## 4.1 Cloud Masking

An evaluation of the overall results show that a total of 1610 scenes were analyzed, that is a median of 35 scenes per sample site over the whole timespan, so more than 5 images per year. **Table 9** shows the precise number of scenes and median scenes per site. If this work would have only used cloud-free images (assumption of a cloudy pixel percentage of less or equal to 10 of the whole sentinel-2 image), this would have only resulted in about 6 scenes per sample site over the whole timespan.

**Table 9:** Number of scenes that were used for calculating the VI's.

| Land Cover Type | Total Scenes | Median N of Scenes per Site |
|---|---|---|
| Forest (n=15) | 514 | 34 |
| Agroforestry (n=16) | 590 | 36 |
| Palm Plantation (n=15) | 506 | 34 |

In **Figure 5**, the process of selecting images is presented visually, at the example of one sample site. Each point represents one available Sentinel-2 image for the here chosen sample site (ID = 111). The line shows the selected CS+ median of 0.6. Red points indicate the images chosen for the final analysis. It can be seen that in some months, several images were available from which the best one was selected. In other months there were no images available at all. It also shows that the number of available images varies strongly between the years, ranging from only 4 images in 2019 and 2022 to as many as 9 images in both 2020 and 2021. The available images were also examined by their cloud cover percentage (an attribute of Sentinel-2 images). In **Figure A. 3:** Sentine-2 images with their respective cloud cover percentage over the whole timespan of analysis that overlap with the sample sites. All sample sites were considered for this plot.**Figure A. 3** (in the Appendix) all the available images across the entire time span and the entire study area (if there was more than one per date, the one with the lowest cloud cover was used) were used to calculate the rolling mean of the cloud-cover percentage are shown. It is evident that several images are almost completely cloud-covered, while few have little to no cloud cover at all. The spread of cloud-cover values appears larger

from June to September. From April to October, more images have a lower cloud-cover percentage. This pattern is also reflected in the rolling mean, which shows an annual cycle with lower cloud coverage between July and September. Peak cloud cover tends to occur between March and April and again around December, although the exact timing of minimal and maximal cloud cover shifts somewhat from year to year. In 2020 and 2023, a small local maximum appears during a period that typically shows the lowest cloud cover (August to September).

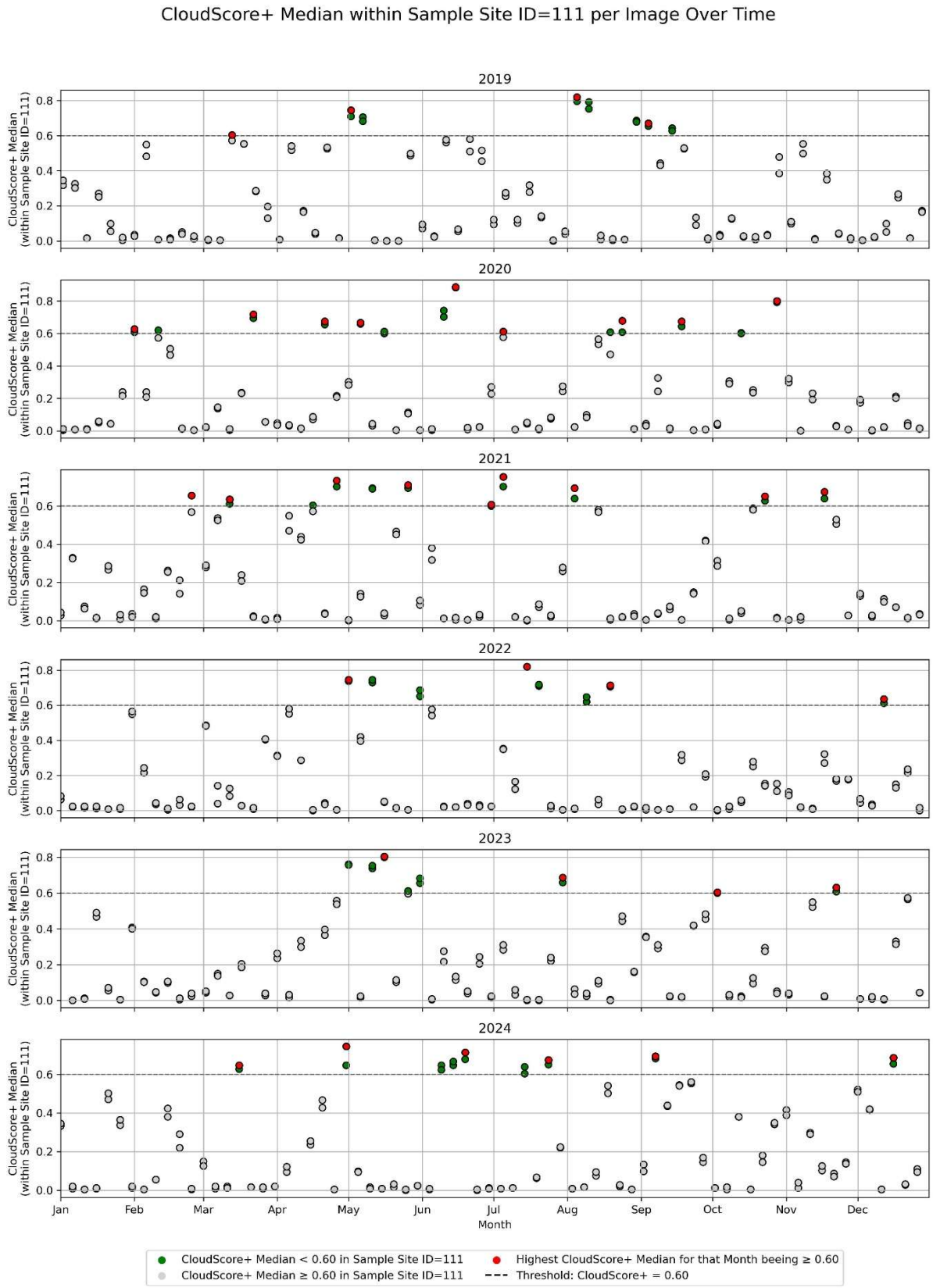


**Figure 5**: Visual example of how cloud masking influenced the choice of images that were processed further in the analysis.

## 4.2 Spectral Indices as Approximation for Functional Traits

The resulting 1610 scenes were analyzed by extracting the mean value of each index over the whole scene.

### 4.2.1 Performance and Comparison of Spectral Indices

At first the results regarding how index values performed and how they related to the land cover categories are presented. Only a selection of boxplots will be provided here, the rest can be found in the Appendix (**Figure A. 4** - **Figure A. 7**). The boxplots in **Figure 6** present the results of the NDVI and the NDRE2 over all years, shown separately for the three analyzed land cover types. The overall pattern across land cover classes remains consistent for all greenness and chlorophyll describing indices. Agroforestry sites generally exhibit lower index values compared to natural forests and oil-palm plantation sites. Forest areas tend to show slightly lower mean values for most indices than palm plantations. Regarding variability, oil-palm plantation sites displays a broader range of values for all indices except EVI and TCARI/OSAVI compared to the other two land cover types. When comparing the indices calculated at the 10 m scale (NDVI and EVI) to those at 20m scale there is no difference in the range of values relative to the other indices.

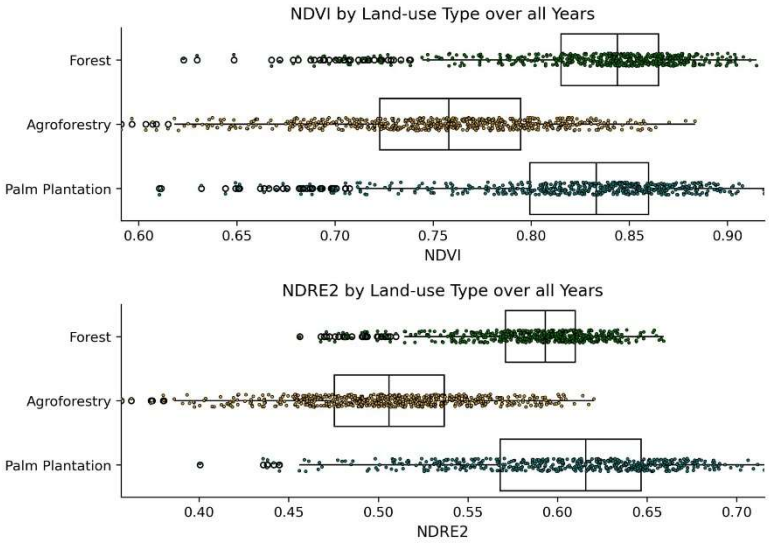


**Figure 6** : Boxplots of NDVI and NDRE2.

The boxplots of water indices show a high consistency in the differences observed between land-use types (see **Figure 7** and **Figure A. 6:** *:* Boxplots of NDWI and NMDI. While chlorophyll-related indices are higher in palm plantations compared to forests, this trend reverses for the water indices. Agroforestry sites consistently show the lowest canopy water content as indicated by the selected indices. Data points for these indices are more compact and show less variability overall. NDWI and NDII exhibit nearly identical patterns in the boxplots. Even if the range of values across indices is generally similar, the MSI displays a slightly broader range, particularly in forested land cover areas. The value ranges for the other two land-use types closely resemble those seen for the NMDI. Notably, there are some quite pronounced outliers toward the lower range for all indices in the palm plantations.

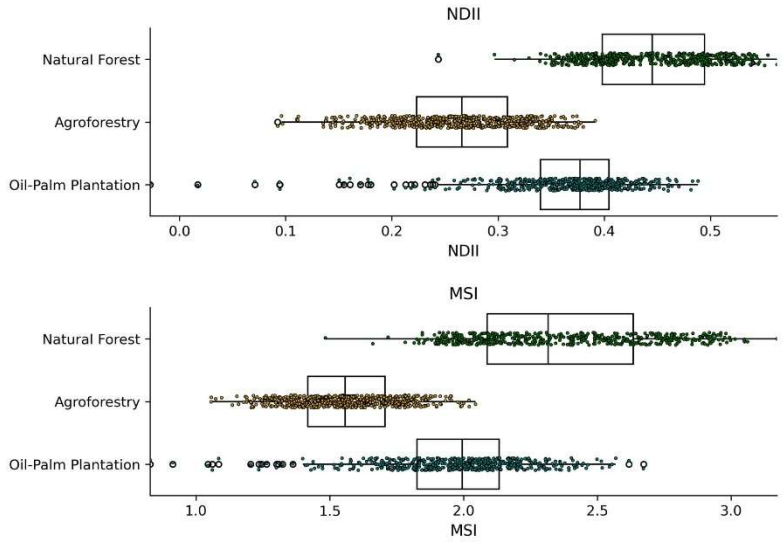


**Figure 7** *:* Boxplots of NDII and MSI

**Figure 8** and **Figure A. 7** presents the indices related to pigments. Both ARI indices (ARI1 and mARI) show very similar values, with higher anthocyanin content detected in forests and palm plantations compared to agroforestry sites. The range of values is slightly broader for mARI than for ARI1. On the other hand, both ARI1 and mARI indices appear unreliable when compared to literature values, suggesting that the data may not be valid for use (Gitelson et al., 2009). The CRI1 index exhibits notable high-value outliers in the forest category, causing a noticeable spread in the boxplots upper quantile. The PSRI index displays a higher mean value in agroforestry compared to forests and palm plantations, accompanied by considerable variability. Despite having a lower mean than agroforestry, palm plantations exhibit upper

outliers comparable to those of agroforestry. In contrast to palm plantations, forests tend to show more outliers on the lower end of the value range.

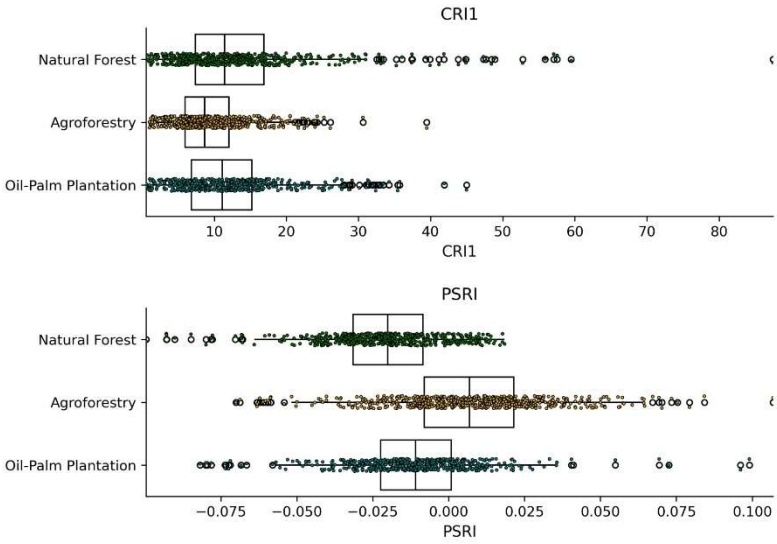


**Figure 8** : Boxplots of CRI and PSRI

The correlation matrix of the tested indices gives more detailed insights into how the individual indices behave. The matrix is shown in **Figure 9**. At first glance, it becomes clear that most indices correlate well with the other indices within the same category. Within the greenness indices, EVI stands out with a remarkably low correlation to NDVI, while OSAVI and NDVI have a strong relationship. When comparing the greenness indices to other index categories, one can see that this pattern is consistent. EVI generally correlates less to all other indices than the NDVI. Within the chlorophyll indices most noticeable are $Cl_{green}$, MTCI and especially TCARI/OSAVI. TCARI/OSAVI even shows a negative correlation with the other chlorophyll indices what suggest that it may not have given reliable results. All the other indices show a very strong relation to each other, with NDRE2 and SeLI even having a perfect correlation (r=1). Similarly, the canopy water describing indices also exhibit a strong correlation among each other. The perfect correlation between NDWI and NDII is not surprising due to their almost identical band combinations. NDMI deviates the most, which is explainable by it being the only index that incorporates the second SWIR band. The pigment estimating indices show a mixed pattern. ARI1, mARI and CRI1 correlate surprisingly well. PSRI on the other hand, only correlates weakly with CRI1, even though both indices should

somehow correlate to carotenoid content. Considering the large CRI1 outliers visible in the boxplots, this suggests that CRI1 may not be providing reliable values.

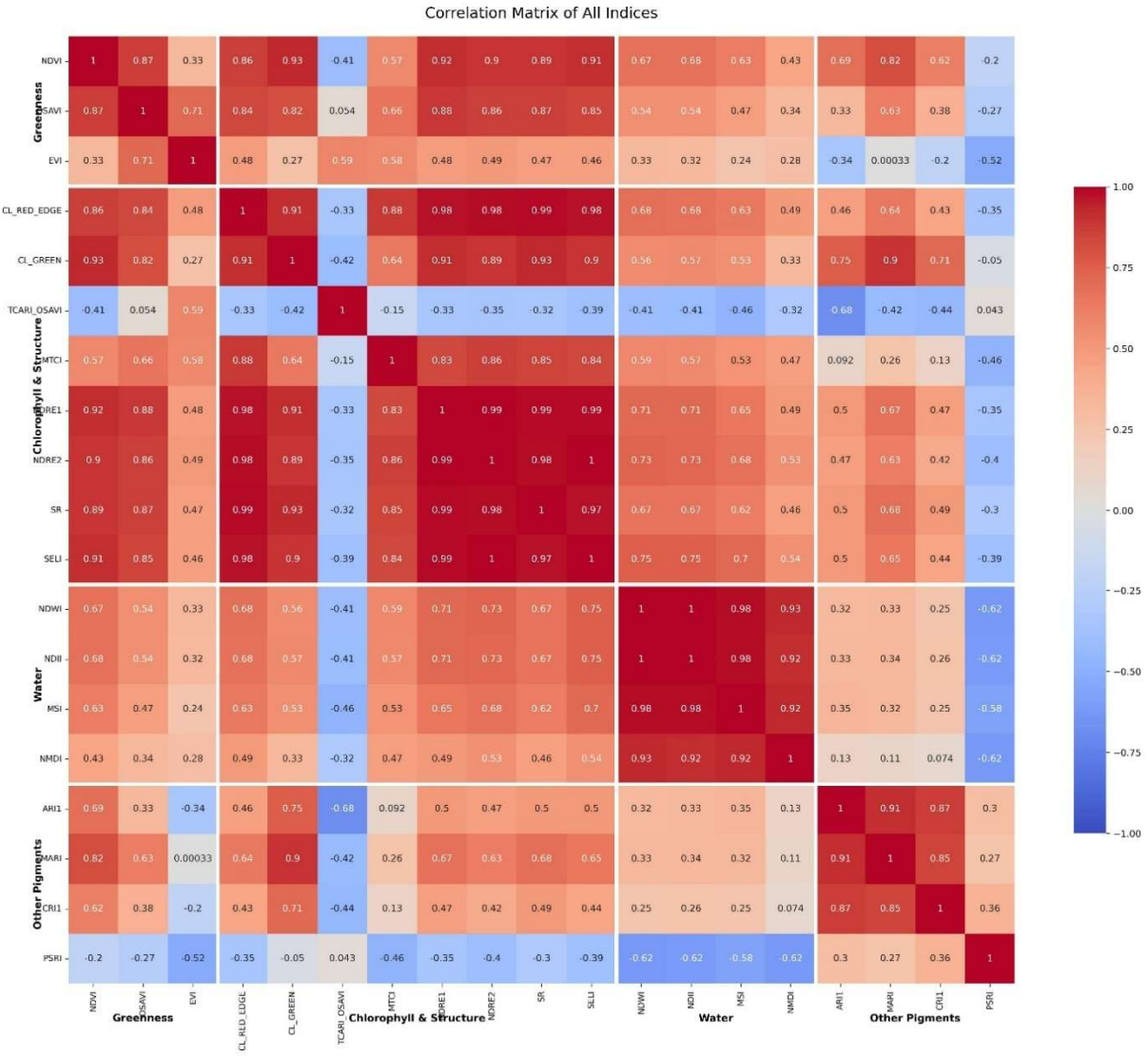


**Figure 9** : Correlation matrix between all calculated spectral indices.

### 4.2.2 Land-Use Patterns of Spectral Indices

The indices were tested on their relationship to the land cover type using a Kruskal-Wallis test. All the indices showed statistically significant relationships with the land-use types ($p<0.05$). **Table 10** shows the p-values per index.

**Table 10** Indices with their respective categories and the p-values from the Kruskal-Wallis tests on the relationship of the index values with the land-cover type are shown.

| Index Name | Category | Kruskal H-value | Kruskal p-value |
|---|---|---|---|
| NDII | Water | 1078.4 | 6.87E-235 |
| NDWI | Water | 1066.3 | 2.82E-232 |
| MSI | Water | 1065.9 | 3.46E-232 |
| NMDI | Water | 869.6 | 1.51E-189 |
| NDRE2 | Chlorophyll | 756.1 | 6.45E-165 |
| SELi | Structure | 754.2 | 1.71E-164 |
| MTCI | Chlorophyll | 750.9 | 8.67E-164 |
| CLred-edge | Chlorophyll | 746.6 | 7.67E-163 |
| NDRE2 | Chlorophyll | 679.6 | 2.62E-148 |
| SR | Chlorophyll | 668.7 | 6.28E-146 |
| NDVI | Greenness | 536.1 | 3.77E-117 |
| Clgreen | Chlorophyll | 486.6 | 2.22E-106 |
| TCARI/OSAVI | Chlorophyll | 422.5 | 1.79E-92 |
| PSRI | Pigment | 389.1 | 3.17E-85 |
| OSAVI | Greenness | 364.6 | 6.57E-80 |
| ARI1 | Pigment | 197.4 | 1.34E-43 |
| mARI | Pigment | 178.4 | 1.82E-39 |
| EVI | Greenness | 177.8 | 2.49E-39 |
| CRI1 | Pigment | 65.3 | 6.73E-15 |

In **Figure 10**, the indices are ordered according to their statistical significance. The x-axis represents the -log10 transformation of the p-values obtained from the Kruskal-Wallis test. This logarithmic transformation was applied to be able to better differentiate between the values, as the raw p-values are all very small. It shows that the significance of the test results is strongly influenced by the category of the respective indices. The four most significant indices are those estimating water content, followed by all chlorophyll-related indices. Lastly,

the pigment-related indices generally show lower significance. Notably, OSAVI and EVI rank among the least significant indices.

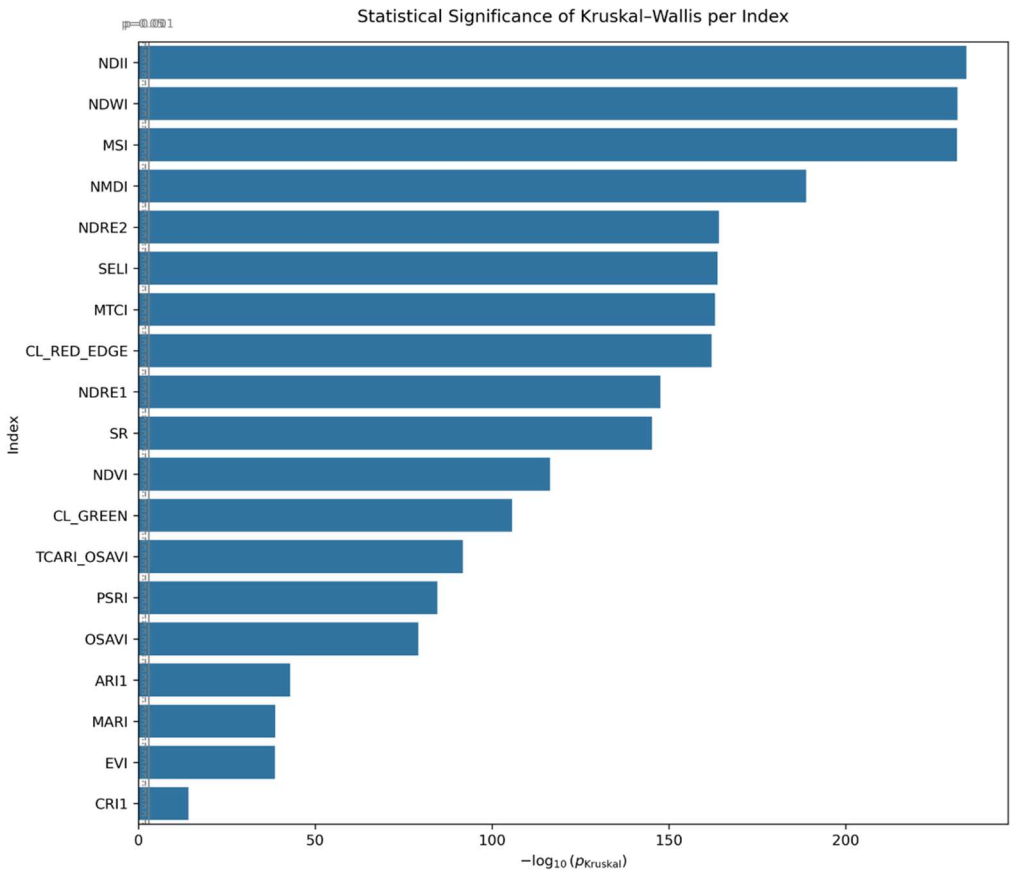


**Figure 10** : Bar plot ranking the indices according to the significance of the Kruskal-Wallis test results. The x-axis shows the -log10 transformation of the raw p-values obtained from the Kruskal-Wallis test. This transformation was applied because the raw p-values are very small and tend to cluster, making it difficult to distinguish differences without scaling.

### 4.2.3 Time Series Analysis of Spectral Indices

The time series of the calculated indices were analyzed collectively to observe how each index developed over time and to assess whether the land-use types differed in their temporal patterns or overall values. Due to the large number of indices, only those showing the most significant differences between land-use types, as indicated in, are presented here. The rest of the time series will just be described.

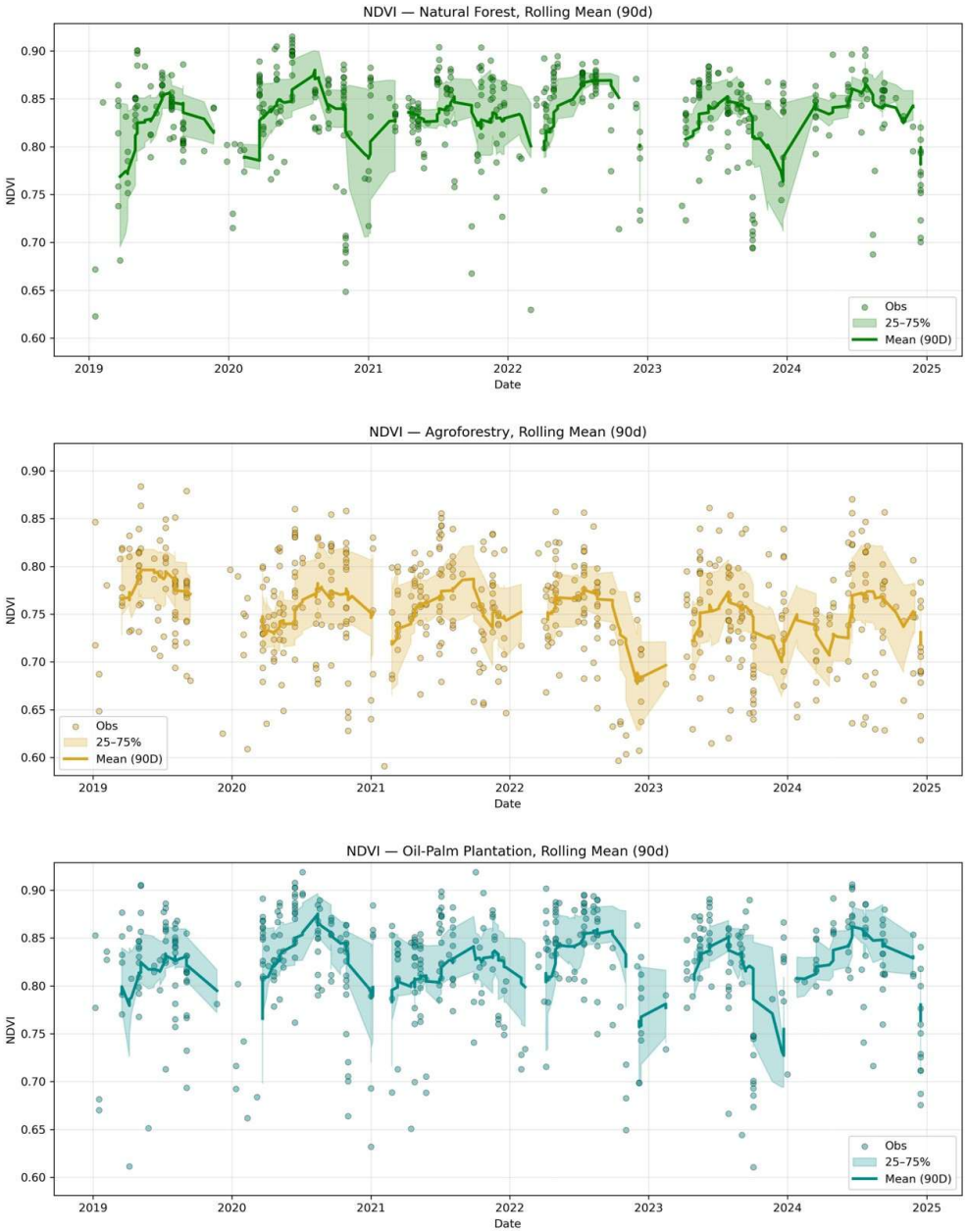


**Figure 11** : Time series of NDVI values over the entire observed period. Points represent individual observations, while the line shows the Gaussian-smoothed median calculated with a 90-day window. The semi-transparent colored bands illustrate the spread between the 25th and 75th quantiles..

For the NDVI (see **Figure 11**), the retrieved values range from 0.6 (with the forest mask value at 0.58) up to 0.92. None of the time series plots show a clear upward or downward trend over the observed period, appearing relatively stable. There is a visible pattern where higher values tend to occur around mid-year (approximately July). This mid-year peak is particularly evident in the forest and palm plantation categories during 2020 and 2024, but less so in 2021 and 2022. A pronounced downward spike appears shortly before 2023 and 2024. The spread of values, represented by the 25th and 75th quantiles, varies over time: the forest category

shows noticeably larger quantile ranges in winter 2021 and 2024, which is partially reflected in the palm plantations as well. The agroforestry time series exhibits a more regular and consistent spread of values throughout the year, with no apparent difference in spread between early and mid-year. The NDRE2 values (shown in **Figure 12**) range from a minimum of 0.35 to a maximum of 0.71. The time series does not exhibit any clear trend over the observed period. Seasonality, which is prominent in the NDVI time series, is less pronounced in NDRE2 but still noticeable. Local maxima appear around mid-year in 2020 and 2022 for the palm plantation land-use category, while local minima occur at the beginning of 2021 and 2024.

Notably, the seasonality is barely visible in the forest category, where the time series appears relatively stable. However, the most prominent outliers occur toward the end of the years. This stability corresponds with the narrow quantile range observed in the forest plots, in contrast to the palm plantations, which display a wider spread of values. The agroforestry time series falls between forest and palm plantation categories in terms of quantile spread. Outliers in the palm plantation category are mostly skewed toward lower values, while they are distributed more regularly around the mean for the agroforestry sample sites. **Figure 13** shows the NDII time series. With a minimum of -0.027 (an erroneous value) and a maximum of 0.56. Just as the other reviewed indices there is no clear trend visible, and here the perceived seasonality also seems to be less prominent. While the values for the forest land-use type are very consistent, both the agroforestry sample sites and the palm plantation sample sites mostly exhibit NDII value outliers to the lower end of the scale. The quantile range seems to be smallest for the natural forest sample sites.

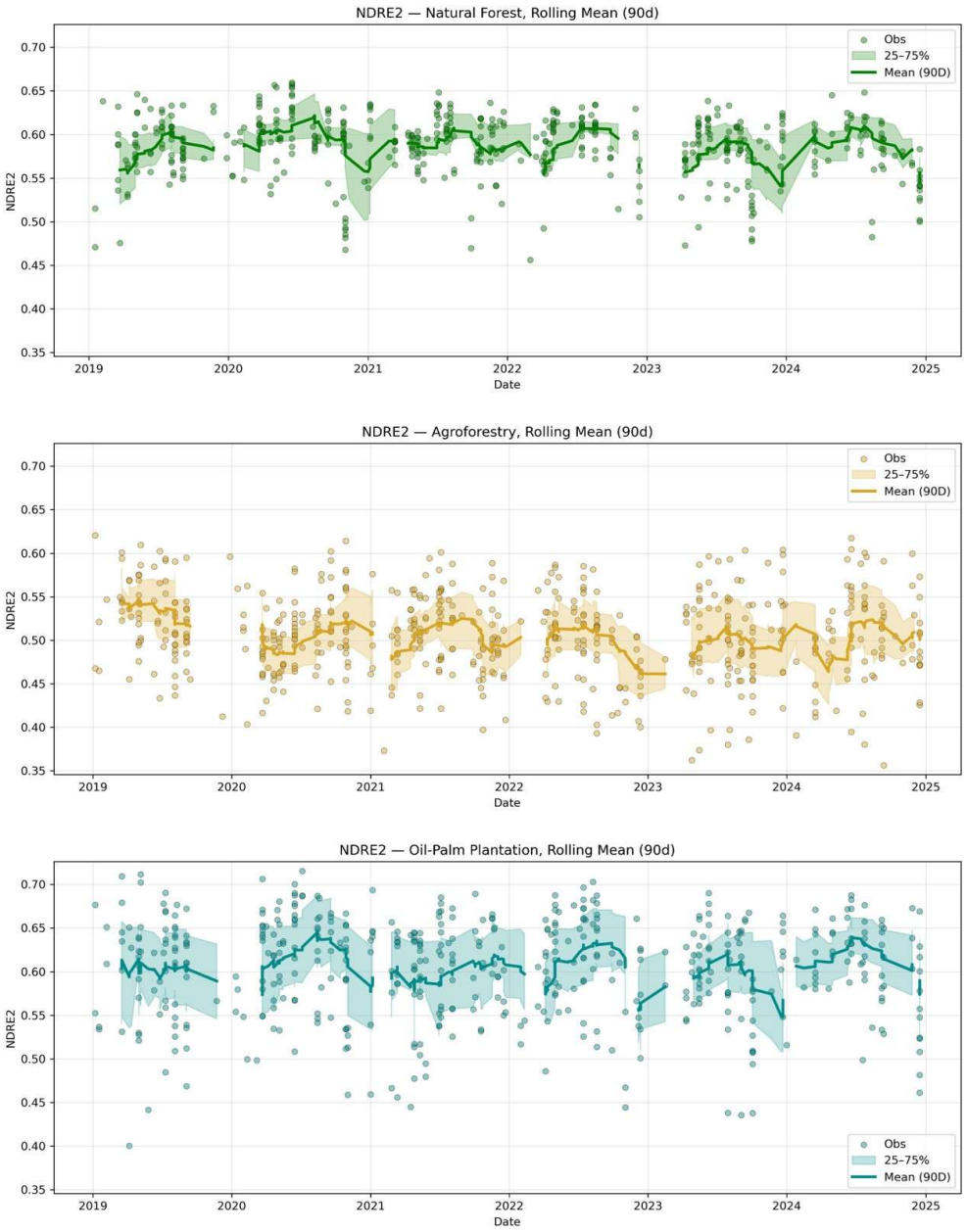


**Figure 12** : Time series of NDRE2 values over the entire observed period. Points represent individual observations, while the line shows the Gaussian-smoothed median calculated with a 90-day window. The semi-transparent colored bands illustrate the spread between the 25th and 75th quantiles.

land-use type again. Finally, the time series of the PSRI is discussed (see **Figure 14**). Values range from -0.099 to 0.11, and no overall trend is apparent. Compared to NDII, the seasonality observed in NDVI and NDRE2 is visible again in PSRI, particularly with local maxima around 2020 and 2022 and a dip in 2024. This dip is accompanied by a slight increase in the quantile range. Otherwise, the quantile spread remains similar across years and land-use types. Again, an overall trend is not visible. But compared to the NDII the seasonality observed in the NDVI and the NDRE2 is visible again. Especially the local maxima

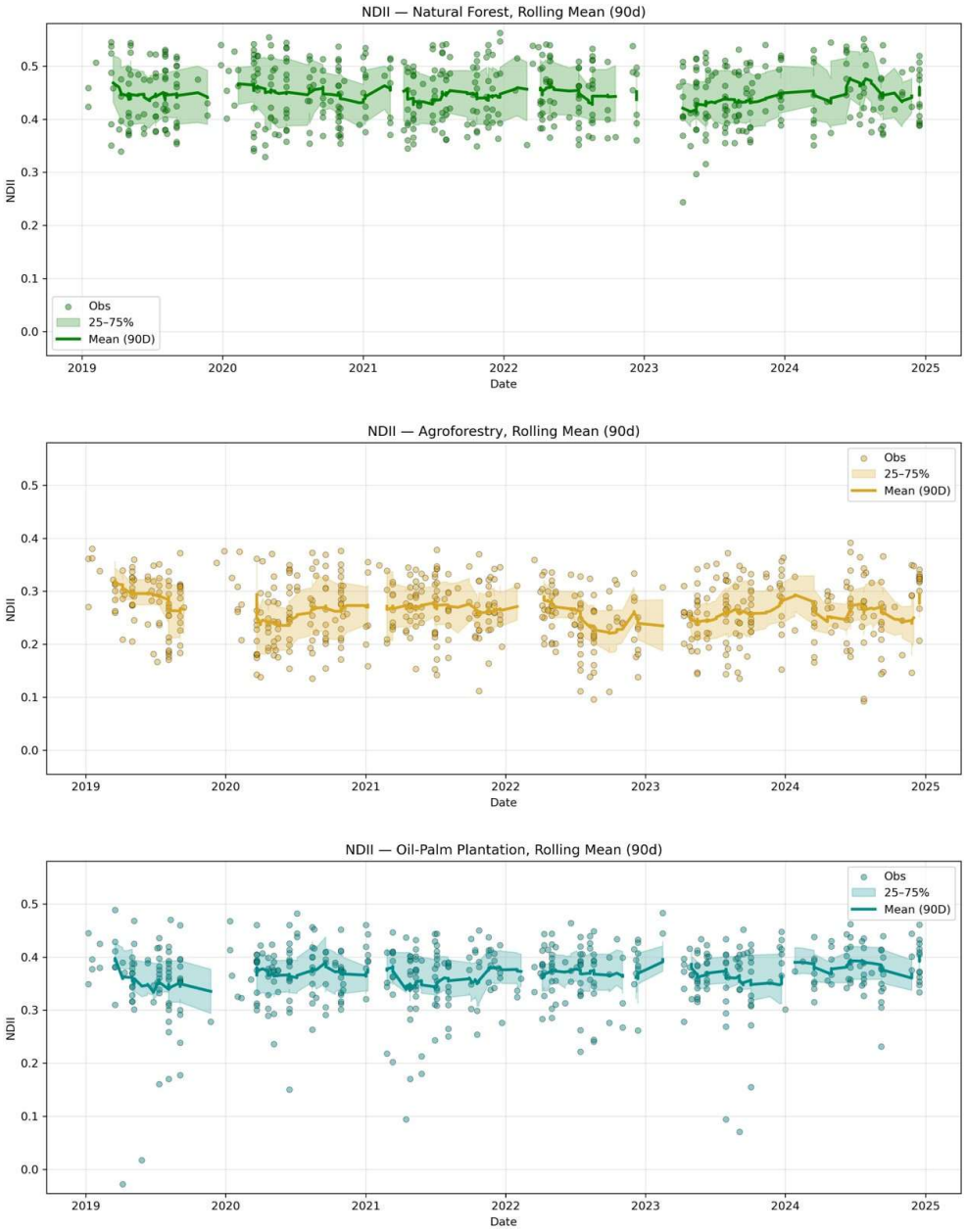


**Figure 13** : Time series of NDII values over the entire observed period. Points represent individual observations, while the line shows the Gaussian-smoothed median calculated with a 90-day window. The semi-transparent colored bands illustrate the spread between the 25th and 75th quantiles.

in 2020 and 2022 and the dip in 2024, where also the range of the quantiles becomes a bit lager. The range of the quantiles is similar for all the years and land-use type otherwise.

The difference between wet and dry season was examined. As already mentioned, the dry season was defined as May to October and the wet season as November to April, for simplicity. A total of 1051 scenes analyzed were during the dry season, compared to only 559 scenes for

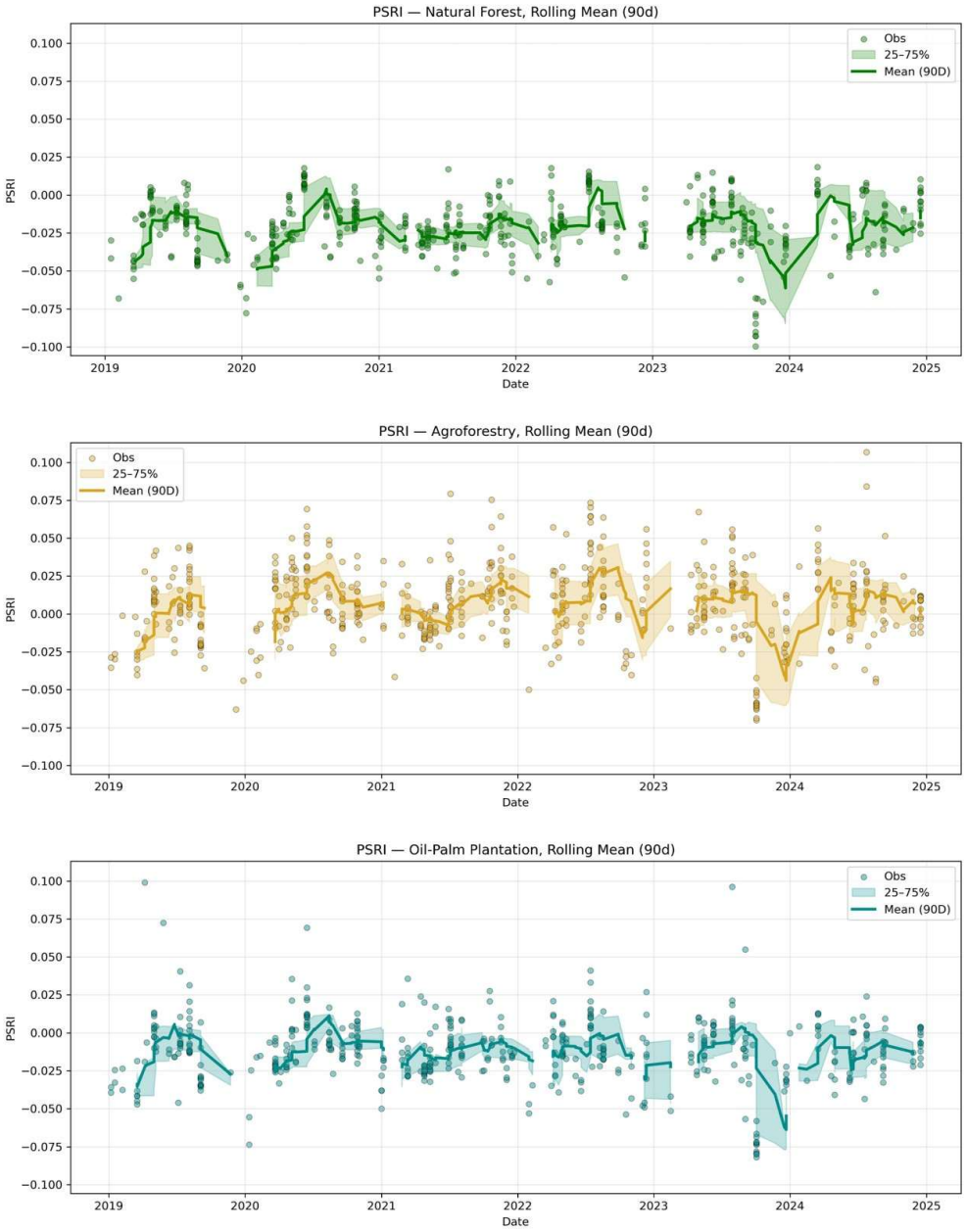


**Figure 14** : Time series of PSRI values over the entire observed period. Points represent individual observations, while the line shows the Gaussian-smoothed median calculated with a 90-day window. The semi-transparent colored bands illustrate the spread between the 25th and 75th quantiles.

the wet season. A Kruskal-Wallis test was applied to assess whether the relationship between season and index values was significant. The results revealed that this relationship indeed is significant for 15 out of 19 indices. Three out of the four indices showing no seasonal relationship were water describing indices, the NDWI, NDII and MSI. The remaining index without a seasonal relationship was the chlorophyll estimating MTCI. Although the NDMI and OSAVI indices showed a significant seasonal relationship, the p-value was higher than those of the other indices with a significant relationship. The indices and their statistical values

are shown in **Table 11**. Besides looking at the relationship between index values and season, the correlation between CS+ median within the sample site and index values was assessed as well. The results are displayed in **Table A. 1** in the appendix. The correlation showed to be significant for all indices except MSI and MTCI. Pearson r values range from 0.062 to 0.548. Seven indices show a Pearson r of over 0.3, the rest has a lower value.

**Table 11** Indices with their respective categories and the p-values from the Kruskal-Wallis test on the relationship of the index values with the season are shown.. The degree of freedom is 1.

| **Index Name** | **Category** | **Kruskal H-value** | **Kruskal p-value** |
|---|---|---|---|
| CRI1 | Pigments | 236.7 | 2.07E-53 |
| ARI1 | Pigments | 210.8 | 9.18E-48 |
| mARI | Pigments | 199.3 | 2.91E-45 |
| $Cl_{green}$ | Chlorophyll | 94.4 | 2.54E-22 |
| NDVI | Greenness | 80.9 | 2.38E-19 |
| PSRI | Chlorophyll | 69.8 | 6.45E-17 |
| TCARI/OSAVI | Chlorophyll | 46.4 | 9.41E-12 |
| NMDI | Water | 28.5 | 9.23E-08 |
| SR | Chlorophyll | 28.3 | 1.03E-07 |
| NDRE1 | Chlorophyll | 27.1 | 1.90E-07 |
| SELi | Structure | 20.1 | 7.31E-06 |
| OSAVI | Greenness | 19.6 | 9.48E-06 |
| $Cl_{red\_edge}$ | Chlorophyll | 18.8 | 1.33E-05 |
| EVI | Greenness | 18.8 | 1.40E-05 |
| NDRE2 | Chlorophyll | 18.1 | 2.06E-05 |
| NDII | Water | 3.1 | 0.08 |
| NDWI | Water | 2.8 | 0.09 |
| MSI | Water | 2.6 | 0.10 |
| MTCI | Chlorophyll | 1.2 | 0.28 |

## 4.3 Functional Diversity Metrics

According to the results presented in section 4.2 the indices NDRE2, NDII and PSRI were selected for calculating the functional diversity metrics. This decision was based on how well they differentiated between the land cover types (**Figure 10**) and because all three showed a weak significance with cloud cover compared to other indices in their category.

After removal of scenes that had less than 28 pixel, the dataset contained 239 agroforestry scenes, 333 forest scenes and 278 palm plantation scenes that were used for the evaluation and statistical testing of the diversity metrics.

### 4.3.1 Land-Use Patterns of Functional Diversity Metrics

**Table 12** shows the standard statistical values for FRic. It is noticeable on first glance that there is a huge difference in median and mean of FRic between the agroforestry scenes and the forest and palm plantation scenes. This is also why the axis of the following plots are not aligned between the agroforestry scenes and the forest and palm plantation scenes.

**Table 12** Mean, median and standard deviation (Std) of FRic values calculated from all scenes that had more than 27 pixels and scaling the results by 1000 for better readability.

| Land Cover Type | Mean | Median | Std |
|---|---|---|---|
| Forest | 0.276 | 0.197 | 0.267 |
| Agroforestry | 1.725 | 1.149 | 1.603 |
| Palm Plantation | 0.347 | 0.302 | 0.281 |

**Table 13** Mean, median and std of FDiv values calculated from all scenes that had more than 27 pixel.

| Land-Use Type | Mean | Median | Std |
|---|---|---|---|
| Forest | 0.734 | 0.734 | 0.032 |
| Agroforestry | 0.694 | 0.693 | 0.034 |
| Palm Plantation | 0.710 | 0.711 | 0.030 |

The FRic values (both mean and median) of the agroforestry sample sites are notably higher than those of the forest and palm plantation sites. Also striking is the large gap between the median and mean, as well as the high standard deviation. Palm plantation sites show the second-highest FRic values, with only a small difference between mean and median. In contrast, the forest sites again display a larger discrepancy between these metrics. The FDiv results (see **Table 13**) are much more balanced across land-use types, with mean and median being almost identical. Forest sites show the highest FDiv values, followed by the palm plantation plots, while agroforestry sites exhibit the lowest values. The standard deviation is almost identical for each of the land-use types.

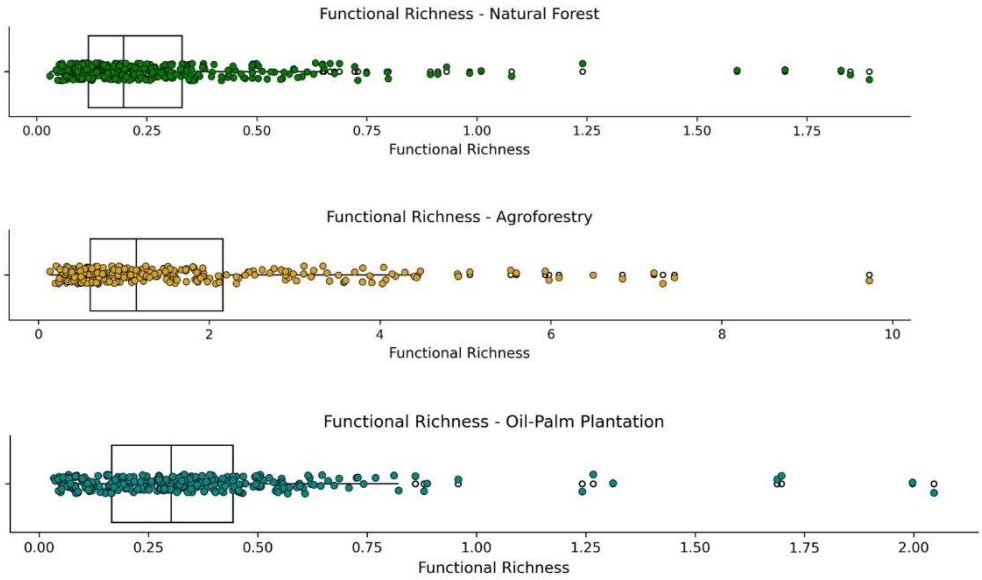


**Figure 15** : Boxplots of FRic values by land cover type. The values are scaled by $10^3$ in order to make the otherwise very small values easier to interpret. The x-axis of the boxplots of the forest land-use type and the palm plantation land-use type were adjusted to each other, while the agroforestry land-use type has its own scale, due to the large difference in value range.

The FRic values can be examined in more detail in **Figure 15**. FRic values were scaled by a factor of 1000 for this plot and all following ones displaying FRic, as it makes the values easier to interpret. This needs to be kept in mind, especially when comparing things like value ranges . Besides the already described mean, the boxplots give additional information about the spread of the data. The interquartile range is shortest for the forest land-use type, followed by the palm plantations. Agroforestry sites show a much larger spread, especially in comparison

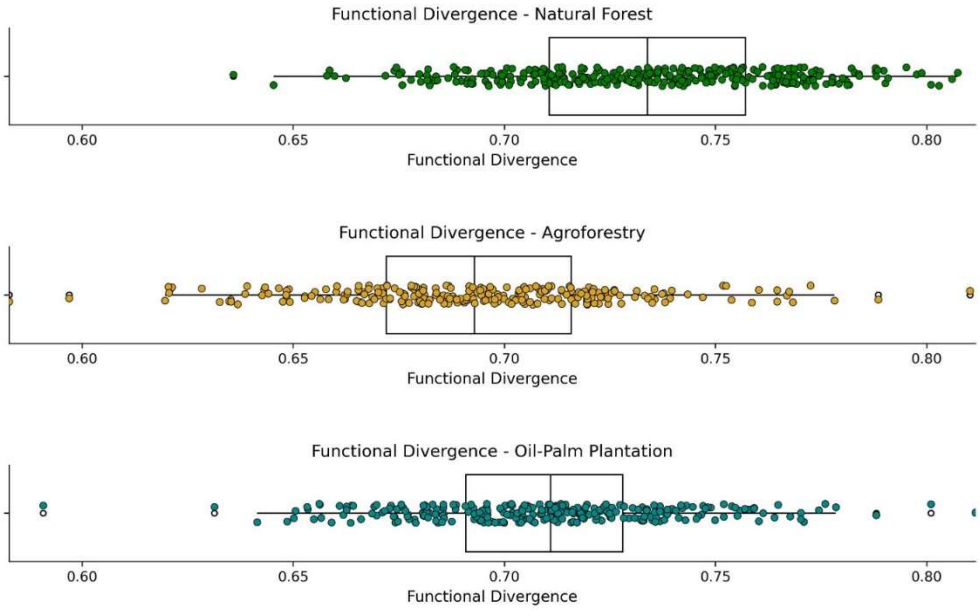


**Figure 16** : Boxplots of FDiv values by land cover type.

to the other two land-use types. It is very noticeable that the values tend to spread further towards the upper range of the data, what is reflected in the larger box size of the third quartile in both the forest and agroforestry boxplots. The palm plantation quantile appears more balanced, although the overall data range shows a tendency towards outliers in the upper values range as well. All this indicate that the value distribution is skewed. The FDiv values (see **Figure 16**) appear much more balanced, with values lying all in a similar range. The forest land-use type has the highest FDiv mean, followed by the palm plantations and then the agroforestry sites. The interquartile range is more balanced and toughly the same size for forest and agroforestry sites, while palm plantations show a smaller interquartile range. Regarding the overall value spread, the distributions appear more regular and also less skewed. The forest sites show a smaller range of values than agroforestry and palm plantations sites, while the latter two have a similar range.

The relationship between the land-use types and the FRic and FDiv values was tested. Both functional diversity metrics were found to be significantly related to the land cover type when testing with Kruskal-Wallis. FRic had an H-value of 379.6 with a p-value of $3.81e^{-83}$ and FDiv had an H-value of 173.5 with a p-value of $2.11e^{-32}$. Compared to a degree of freedom of 2 the results are unambiguous.

### 4.3.2 Time Series of Functional Diversity Metrics

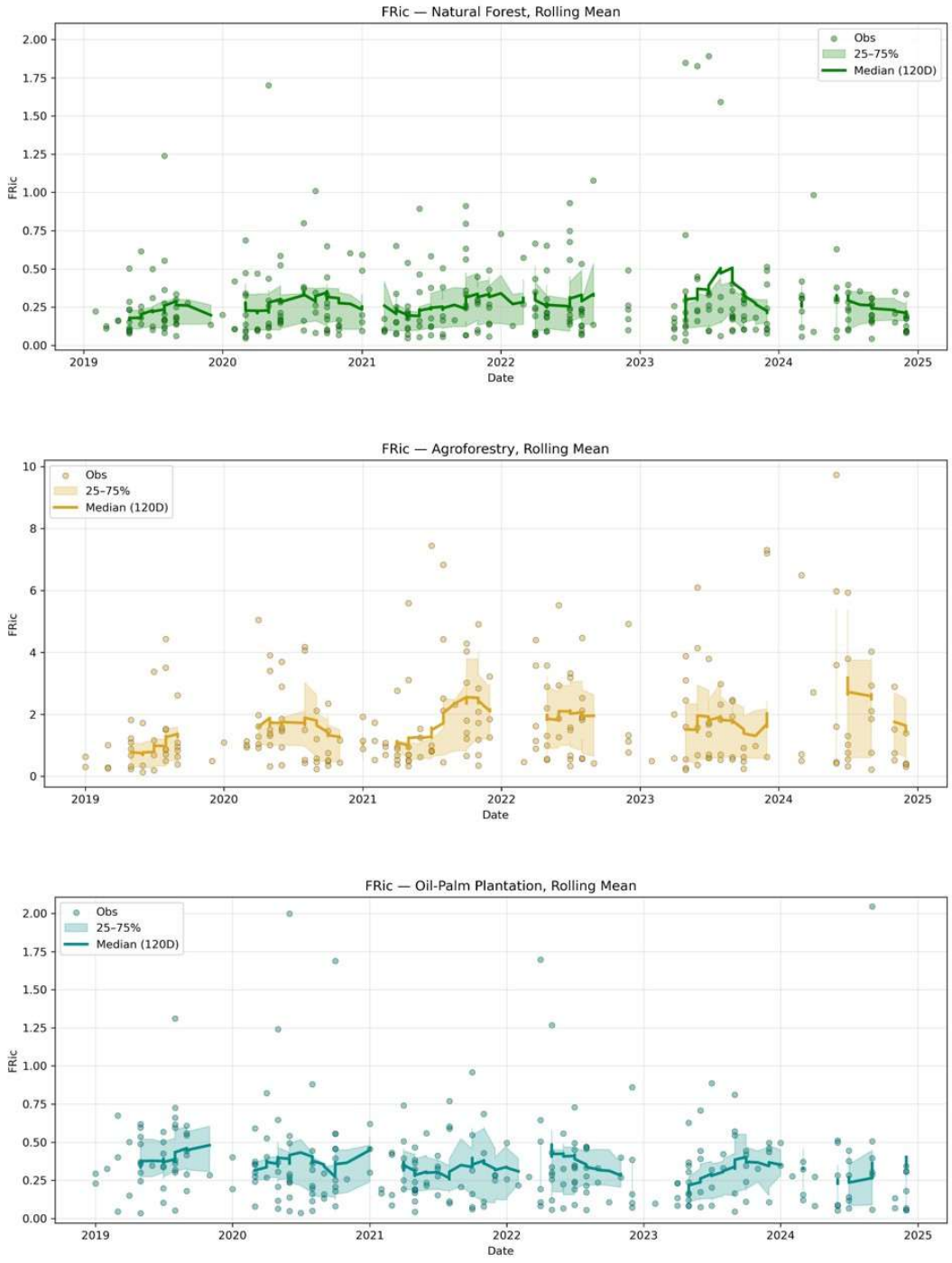


**Figure 17** : Functional Richness time series with a 120d rolling median. Functional richness values are scaled by 1000, as the normal values are very small.

**Figure 17** shows the functional richness time-series values for all land-cover classes, scaled by 1000 for better readability. Similar to the boxplot statistics, the large differences in value

ranges across land-cover types are striking, and all classes show a broad overall spread. Ignoring the absolute ranges, on can see that the time series for the forest and palm-plantation land-use types are much flatter than those of agroforestry. The forest land-cover type has some extreme outliers in 2023, palm plantations in 2020 and 2024 and agroforestry in 2021 and 2024.

No seasonality is visible for any of the land-cover types. This is likely due to the small number of datapoints, especially in the wet season. No meaningful trend can be identified for any of the land-cover types. While fluctuations occur, they are not consistent across categories. For example, in the last third of 2020, both forest and agroforestry show an increase in functional richness, whereas palm plantations exhibit a drop. Moreover, the interpretation is complicated by the fact that the rolling median cannot be calculated during several periods, making it potentially misleading in those sections. Overall, the data contain considerable noise due to the wide spread and irregular of values.

The time series of FDiv appears much more even compared to FRic. As already indicated by the boxplots, the value ranges are similar across all land-cover types. Forest show the highest FDiv values and agroforestry the lowest. The ranges also seem more consistent than those of FRic, particularly for the forest plots. One noticeable exception is an outlier in mid-2021 in the oil-palm-plantation plots. In the agroforestry plots, the range appears to increase from year to year, with the upper-value outliers in particular showing an almost continuous upward trend. As with FRic, no clear trend can be identified overall, which may again be due to noise and the messy structure of the data. There is also no distinct seasonality, although some patterns give the impression that it might be present, especially when looking at the forest and palm plantation time series. However, these patterns are unintuitive: they do not align with the wet or dry season and even appear inverted between forest and palm plantation plots. For example, there is a local minimum at the beginning of 2021 in the forest data, while the palm plantation data shows a local maximum at the same time. Although fluctuations in range are present, the FDiv time series appears more stable than the FRic series. In the forest plots, outliers seem to be distributed more or less evenly around the median, while the agroforestry plots, outliers are clearly concentrated towards the upper end of the value range. The difference between the wet and dry seasons was also examined statistically for the

functional diversity metrics. Again, the Kruskal-Wallis test was used. The p-value for FRic is p=0.024, with an H-value of 5.73 and for FDiv the p-value p=0.255 with an H-value of 1.29, compared to a degree of freedom of 1. Therefore, only FRic shows a statistically significant relationship with the season.

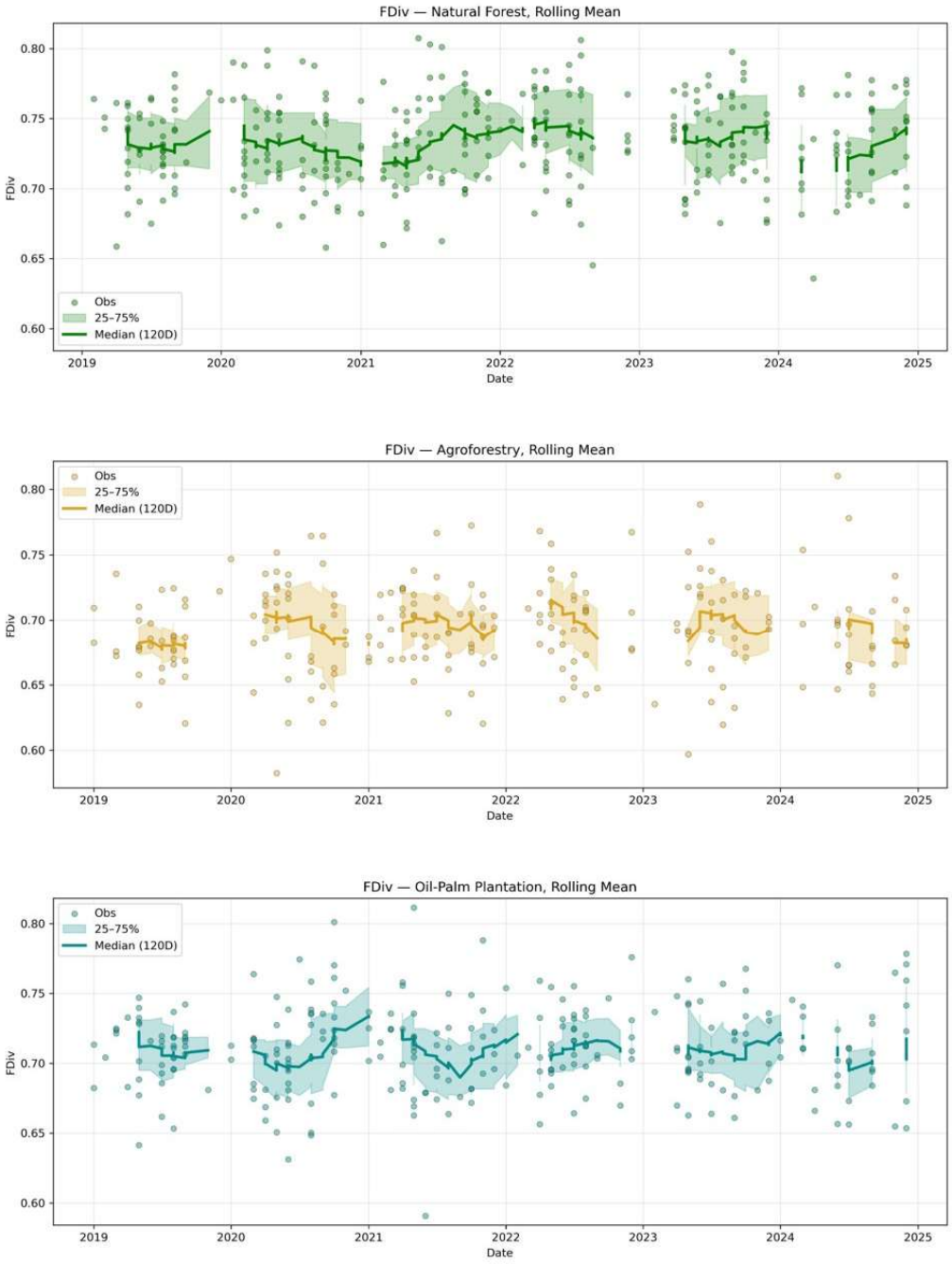


**Figure 18** *:* Functional Divergence time series with a 120d rolling median

# 5 Discussion

## 5.1 Cloud Masking

A frequently discussed key limitation of remote sensing for tropical regions is the high amount of cloud cover that poses challenges as it leads to a limited amount of usable satellite scenes (Mederer et al., 2025). In this study however, the cloud-free data availability per sample site could be increased by cloud masking. This results in having more datapoints across the analyzed timespan and consequently a better temporal coverage. This also allowed to see seasonal patterns in the tested spectral indices.

When cloud-cover patterns, a clear annual cycle becomes apparent, as previously shown in section 4.1 and as illustrated in **Figure A. 3**. Peak cloud cover typically occurs between January and April, whereas the lower levels are observed between June and November. This pattern aligns broadly with the regional wet-dry monsoon dynamics. The correlations between the CS+ medians of polygons and the various spectral indices provide another insight in this regard. All indices, except for EVI, MSI, NDII, NDWI NMDI and TCARI/OSAVI (so foremost water describing indices), showed a rather weak (a Pearson $r < 0.3$) to moderate (Pearson $r < 0.6$) correlation with cloud cover. While this could just be related to the seasonality it might also suggest that there could be a bias in index behavior introduced by cloud cover residues. Distinguishing between these two sources of variability is an open question, but important to understand.

Therefore the next point to discuss is the choice of the CS+ threshold of 0.6 for cloud masking. While the CS+ layer is known for a high accuracy, even small misclassifications or choosing the threshold value too low might have interfered with the index calculations. Choosing a more conservative threshold, or another cloud masking strategy needs to be considered for future works

## 5.2 Vegetation Indices as Approximation for Functional Traits

### 5.2.1 Performance and Comparison of Indices

The correlations among the selected indices, presented in section 4.2.1, provide important insights into their performance and suitability for this study. Overall, most indices behaved as expected, though not all. Within the greenness-index group, the weak correlation between EVI and NDVI is unexpected. In principle, EVI should reduce the influence of soil background and mitigate NDVI's tendency to saturate in dense vegetation canopies. However, EVI also showed lower correlations with several chlorophyll-related indices. This pattern may indicate that, under the conditions of this study area, NDVI captures vegetation variation more consistently than EVI. Within the chlorophyll and structure-related indices, TCARI/OSAVI appears as a clear outlier, showing weak and even negative correlations with all other chlorophyll indices. Besides TCARI/OSAVI, the remaining chlorophyll indices show very high intercorrelations. $CL_{green}$ and MTCI correlate less strongly with the others, likely due to their incorporation of additional spectral bands.

The water-related indices show near-perfect correlations with one another, which is unsurprising given that they are mostly based on the same combinations of bands. The only exception is NMDI, which differs probably because it, as the only index, incorporates the SWIR2 band. Interestingly, NMDI was also the only water index showing a relationship with the wet and dry season. As discussed in section 3.4.3, wavelengths around 1940 nm are more sensitive to atmospheric water vapor absorption due to low solar irradiance (Sims and Gamon, 2003). The broad 175 nm bandwidth of the corresponding Sentinel-2 band may reduce the reliability of this index further. These considerations could explain why NMDI behaves differently from the other water indices, although without validation data this remains speculative.

The pigment indices were the most inconsistent group. According to literature expectations, both ARI1 and mARI produced values that appear unreliable (Gitelson et al., 2009). The underlying reasons remain unclear. Both indices correlate strongly with CRI1, which itself seems to perform more reliably overall. PSRI showed an inverse relationship with most other

indices, which is consistent with its interpretation: lower PSRI values generally indicate less leaf aging and therefore healthier vegetation (Merzlyak et al., 1999). However, the relatively weak relationship between CRI1 and PSRI is surprising, given that both indices should at least partially reflect canopy carotenoid content. This discrepancy suggests that pigment describing indices may be more sensitive to subtle variations in canopy structure, leaf phenology, or illumination conditions than greenness or chlorophyll describing indices., what also matches findings in literature as mentioned in section 3.4.4.

Ultimately, the choice of indices used to calculate the functional diversity metrics, NDRE2, NDII and PSRI was guided by the strength of their relationship with the land-cover types and by how strongly they correlated with the cloud cover.

### 5.2.2 Land Cover Patterns of Indices

Besides looking at correlations among the indices themselves, it has to be considered how the calculated index values relate to the different land-cover types. Rather than discussing every index individually, the focus here is on the broader patterns that emerged. For the chlorophyll-related indices, relatively a consistent pattern was observed. Palm plantations showed the highest values, followed by natural forest, with agroforestry sample sites exhibiting the lowest values. Higher chlorophyll values in palm plantations are well supported in the literature, as oil palm typically have a higher photosynthetic productivity compared to many natural forests. A study from Sabah, Borneo for example reported carbon-sequestration rates that were 60 – 70% higher in oil-palm plantations than in normal forests (Fowler et al., 2011; Murphy, 2024). The lower chlorophyll values observed in the reforested agroforestry sites are likely linked to their developmental stage. As these plots are still growing, canopy density and overall productivity likely remain lower than in a mature forest or in plantation systems. Moreover, growth trajectories vary depending on how the reforestation was approached, what trees were planted and other external factors (Pansit and Parilla, 2024).

For the water-related indices, the pattern was reversed. Oil-palm plantations showed lower values than natural forests, while agroforestry sample sites again exhibited the lowest values. This aligns well with findings in the literature on water dynamics in palm plantations

compared to lowland tropical rainforests. Studies from Kalimantan have shown that oil-palm plantations use 15–20% more water annually than natural lowland forests, primarily due to higher evapotranspiration rates (Fan et al., 2019). The comparatively low water-content values observed in the agroforestry sites can likely be attributed to their still-recovering canopy structure. Additionally, canopy water content is known to be negatively affected by soil background influence, which becomes more pronounced in more open canopies, what can be expected in reforested areas (Cheng et al., 2006).

For the pigment indices, interpretation is limited to CRI1 and PSRI, as the other indices produced unreliable values. CRI1 was highest in natural forest plots, closely followed by oil-palm plantations. Although the mean values of forests and plantations were similar, forest sites exhibited a greater number of high outliers. This could indicate more heterogeneous canopy conditions in naturally forested areas, though this cannot be confirmed on the basis of this result. PSRI showed an inverse pattern, with agroforestry plots displaying the highest values and natural forests the lowest. Since lower PSRI values typically indicate reduced leaf senescence and lower stress levels, the natural forest's low PSRI is consistent with healthier canopy conditions. Palm plantations, on the other hand, are known to be rather sensitive to environmental fluctuations and generally exhibit lower resilience to stressors such as temperature shifts or water limitation, which may explain their lower PSRI values (Rubilar et al., 2024).

### 5.2.3 Temporal Patterns of Index Values

The temporal pattern of the index values was presented in section 4.2.3. Again only the three indices that were consecutively used for the functional diversity metrics calculations will be discussed.

Broadly speaking, none of the calculated indices shows a clear long-term trend across the entire study period. While this was probably to be expected for oil-palm plantations and natural forests, it also indicates that no substantial change has occurred yet in the agroforestry sample sites. Reforestation in these plots only began in October and November 2022, which leaves just two years within the analyzed time series for any measurable effects to appear. It is also known that the sample sites differed in their initial conditions when reforestation started,

meaning they had varying vegetation cover before the reforestation, which may partly explain the lack of a consistent signal. Additionally, some plots may have experienced setbacks or unsuccessful early establishment phases. Ultimately, it is very likely that the monitoring period is simply too short to detect clear improvements. The absence of trends in oil-palm plantations and natural forests is more straightforward to interpret. Palm plantations typically follow a life cycle of more than 25 years, and natural forests can persist for much longer if not affected by external disturbances (Murphy et al., 2021).

Although no long-term trends were detectable, all indices showed a clear seasonality. This is visible in the time-series plots in section 4.2.3, where most indices exhibit higher values about during the dry season and lower values during the wet season. This also reflects the statistical results presented in **Table 11**, where many index values were significantly related to the wet and dry season. Three of the four indices that did not show a significant relationship with seasonality were water-related indices, namely the NDII, NDWI and the MSI. At first glance, this was surprising, as the tropics are often described as relatively aseasonal due to their stable temperatures throughout the year (Mederer et al., 2025). But work from the Amazon Basin has shown a pattern, with increased photosynthetic activity during the dry season, what is an effect often attributed to higher sunlight availability when cloud cover decreases. Bi et al. (2015),, for example, describe seasonal variations in the Amazonian rainforests and report "dry-season greening" driven by more irradiance due to less cloud cover. This latter pattern corresponds more closely to what is observed in our dataset These findings suggest that in Borneo, water might not be a limiting factor for most of the year, which would explain why three of the four water indices showed no relation with the seasonality. Only NMDI deviated from this pattern, which was already addressed in the previous subsection. The only non-water index that did not correlate with seasonality was MTCI, a chlorophyll-related index. MTCI is the only index that includes the 665 nm band, which lies just below the red-edge region. Since all other chlorophyll indices did show seasonal patterns, this may indicate that MTCI is less sensitive to chlorophyll changes under these conditions.

The pigment describing indices all showed seasonality. Although this may seem counterintuitive, especially for PSRI, which is associated with leaf senescence and stress, both

CRI1 and PSRI partially reflect carotenoid content. Carotenoids act as photoprotective compounds, so an increase during periods of higher sunlight intensity might be plausible and consistent with the patterns observed in this study (Hashimoto et al., 2016).

The observed seasonality suggests that monitoring efforts need to account for the time of year, since index values taken in different seasons may reflect seasonal dynamics rather than actual change.

## 5.3 Functional Diversity Metrics

### 5.3.1 Land Cover Patterns of Functional Diversity Metrics

The FRic values, calculated from NDRE2, NDII, and PSRI, showed a highly unexpected distribution across land-use types. As presented in section 4.3, the agroforestry sample sites exhibited FRic values roughly five times higher than those of natural forest and oil-palm-plantation sites. Based on previous studies, the expectation was that values would be more similar across land-cover types, and that the ranking would follow more intuitive results, e.g., that natural forest sample sites yield the highest FRic values. However, the results obtained here contrast with the patterns reported in literature. From a theoretical standpoint, forests would be expected to have the highest FRic, given their typically high functional and chemical diversity. For example, Asner et al. (2012) found that Dipterocarpaceae, which are dominating the lowland Bornean forests, exhibit as much chemical variation among species as all other tree families combined in their study. Hauser et al. (2022) found that palm plantations showed significantly lower functional richness than both intact and logged forests, so findings that align with ecological expectations for lowland tropical forests. In this analysis, by contrast, the agroforestry sites displayed extremely high FRic values, and palm-plantation FRic values exceeded those of forests. To better understand this pattern, some of the agroforestry sites with extreme values were examined in detail. An example is shown in **Figure 19**, illustrating the agroforestry sample site 109 on 19 June 2024, alongside a PlanetScope image from 15 June 2019 for reference. Two observations stand out.

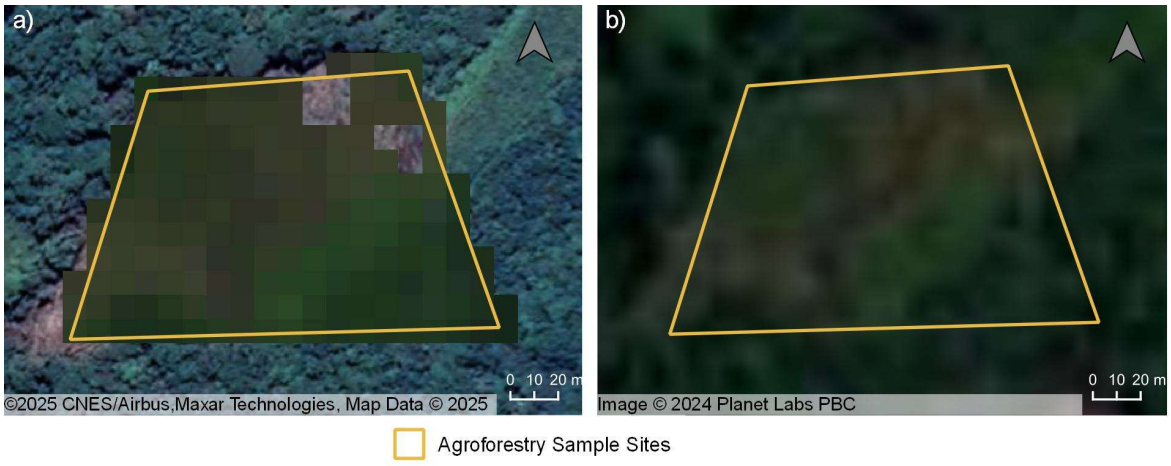


**Figure 19** : Example of Agroforestry Sample Site with a high FRic value.

First, the polygon appears to extend across multiple land-cover types. The lower-right section shows substantially denser vegetation than other parts. Second, a brownish coloration in the polygon's center suggests either damaged vegetation or substantial soil influence. Notably, the NDVI-based forest mask did not exclude these brownish pixels. Although this cannot be confirmed for all sites, such mixed-pixel effects provide a plausible explanation for some of the extremely high FRic values. One contributing factor may be the relatively small polygon size. This interpretation is supported by a recent work from Helfenstein (2024), who showed that mixed-pixel problems increase when pixel size approaches the size of the object being observed, in this case the sample sites. The findings also demonstrated that mixed pixels at coarser spatial resolution tend to decrease FRic values, and that polygons located near forest edges may be especially sensitive to external influences. A similar explanation may apply to the unexpectedly high FRic values observed in palm-plantation sites relative to forests. In Hauser et al. (2022), plot sizes were approximately 40 ha, what is substantially larger than the 1.1 ha plot sizes used in this study. In addition, palm-plantation canopies tend to be more open than forest canopies, which may amplify mixed-pixel effects in the plantation sites (Khokthong et al., 2019). Thus, the FRic values observed here are likely influenced by spatial-resolution limitations, polygon size, and canopy heterogeneity and do not reflect the real FRic differences between the land-use types.

In contrast to the FRic values, the FDiv results show a pattern and value range that more closely align with ecological expectations. Natural forests exhibit the highest FDiv values,

followed by oil-palm plantations, while the agroforestry sites show the lowest functional divergence. The distributions appear relatively balanced across land-use types, although palm-plantation and agroforestry plots display more outliers than the forest sites. Because FDiv reflects how communities are distributed within trait space, it provides insight into ecological differentiation and the distinctness of functional roles within a community. Higher FDiv is typically associated with greater niche specialization. It is therefore plausible that forests, show higher functional divergence than palm plantations. This interpretation is consistent with the findings of Hauser et al. (2022), who likewise reported higher FDiv in natural forests than in plantation systems. The lower FDiv values observed for the agroforestry plots may at first seem counterintuitive, as reforestation does not necessarily rely on planting a single species. One possible explanation is the early developmental stage of these reforested areas: young planted trees may still share relatively similar trait expressions, with greater functional differentiation emerging only over time. A second, and perhaps more plausible, explanation relates to methodological effects. As noted by Helfenstein et al. (2024), mixed-pixel issues, even though they are less influential for FDiv than for FRic, tend to reduce FDiv values at coarser spatial resolutions. Given the probably relatively open canopies and residual soil visibility in many agroforestry sites, such effects may have artificially lowered their FDiv estimates. This remains a hypothesis, however, and was not explicitly tested in this study.

### 5.3.2 Temporal Patterns of Functional Diversity Metrics

The time series of the FRic values is shown in section 4.3.2 **Figure 17**. There is no clear long-term trend in any of the land-cover types. Seasonality is only faintly visible in the plots but turned out to be statistically significant based on the Kruskal–Wallis test. The absence of a trend can have several explanations. For natural forests and palm plantations, both long-lived and slowly changing ecological systems, a lack of trend is not surprising. For the agroforestry sites, however, a development toward the forest values might have been expected. Because of the previously discussed mixed-pixel effects and other issues that produced extremely high agroforestry FRic values, it is difficult to determine whether a trend is truly absent. It is possible that polygons with less soil influence would have shown a clearer pattern, but the method used here did not reliably handle soil-affected pixels. With such high noise levels, any existing trends probably is obscured. Although the statistical test indicated seasonality, the

visual impression remains weak. This is largely due to gaps in the dataset, which were further increased because sample sites with fewer than 28 pixels had to be removed. As a result, the statistical power of the test is likely limited. Based on the time-series plots alone, it is difficult to determine what drives the seasonal signal. It could be related to the dry-season greening described earlier, but with the small number of observations it could also be influenced by cloud cover residuals. With the available data, it is not possible to clearly separate seasonality from methodological artefacts.

The FDiv time series is shown in **Figure 18**. Similar to FRic, no long-term trend is apparent. In contrast to FRic, however, no seasonality is visible—neither visually nor statistically. The absence of a trend likely has the same explanation as for FRic, tree-based systems change slowly, and small ecological shifts are not immediately reflected in structural metrics. Methodologically, FDiv is more stable than FRic, which is evident from the more evenly distributed outliers around the mean in the time-series plot. An interesting question is why FDiv did not show seasonality while FRic did. Several explanations are possible. One is that the data were simply too noisy for a seasonal pattern to be detected, given the many gaps and the variable noise levels, especially in the agroforestry plots. Another possibility is ecological: even if FRic increased during seasonal greening (e.g., higher NDRE2 values), the relative distribution of traits might have remained stable. In other words, trees occupying similar ecological niches may have remained clustered in trait space, preventing changes in FDiv. This would support previous findings that FRic is more sensitive to external influences than FDiv (Helfenstein, 2024). However, as with the FRic time series, interpretation must remain cautious due to the limited number of observations and the uneven temporal spacing between them.

## 5.4 Limitations

Several methodological and ecological factors should be considered when interpreting the results of this study, particularly regarding data quality, polygon size and the sensitivity of the functional diversity metrics.

### 5.4.1 Cloud Masking

This study relied on cloud-masking rather than using only cloud-free satellite scenes. While this approach increased the number of usable scenes, the analysis showed a relationship between index values and cloud cover. This might indicate a trade-off: although more data was available, some scenes might have been insufficiently cloud-masked what can be leading to noise.

### 5.4.2 Sample Site Size and Quality

The small spatial extent and precision of the sample sites proved to be a substantial limitation. During preprocessing, the agroforestry sample sites had to be buffered because the original sample sites were too small to calculate functional diversity metrics by the findings of Helfenstein (2022). This likely resulted in some polygons incorporating neighboring land-cover types again, such as roads or parts of plantations. Even after buffering, a majority of the agroforestry sample sites remained only marginally large enough for functional diversity calculations. Small polygons are particularly vulnerable to mixed-pixel artefacts and boundary noise, which can alter both index values and trait-space metrics. Functional richness (FRic) was especially sensitive to these effects, as it expands strongly in response to even a few extreme pixels (Helfenstein et al., 2022) . Occasional overlaps with adjacent land-cover types, even if they were tried to me mitigated by shifting the agroforestry sample sites, may have introduced spectral heterogeneity unrelated to the target vegetation.

### 5.4.3 Index Accuracy for Canopies

While many indices performed ecologically plausibly, the limitations of optical indices at canopy scale must be acknowledged. As noted by Huang et al. (2015), pigment-related indices are particularly prone to constraints caused by canopy saturation, shadowing, and scattering, which can weaken their sensitivity to traits. Thus, some of the observed variability may reflect structural or illumination effects rather than true differences in values.

### 5.4.4 Temporal Extent of the Analysis

Finally, the temporal extent of the study presents a constraint. Although six years of imagery were analyzed, reforestation of the agroforestry sites began only late 2022. This

provides just over two years to detect changes and is likely too short for meaningful shifts, especially given differences in initial vegetation between plots. As a result, the absence of clear temporal trends should be interpreted cautiously.

# 6 Conclusion

This thesis aimed to evaluate the potential of trait-describing spectral indices and functional diversity metrics for long-term biodiversity monitoring in a tropical region with high cloud cover. Specifically, it addressed how high cloud cover affects per sample site cloud-free data availability for long-term monitoring, which temporal patterns emerge within and between land-cover types, how multiple indices can be combined to complement each other, and which indices or traits are most suitable for continuous monitoring.

Dealing with cloud cover proved to be a challenge. Rather than relying exclusively on cloud-free images, this study applied cloud masking to all available scenes. This approach substantially increased the cloud-free data availability, yielding on average more than five usable images per sample site per year, so more than would have been possible with a cloud-free-only strategy. Additionally, the shorter temporal intervals between scenes enabled the detection of seasonal patterns.

Regarding seasonal patterns, most spectral indices displayed a significant relationship to wet and dry seasons.. A consistent increase in greenness- and chlorophyll-related indices during the dry season suggests patterns similar to the "dry-season greening" described for Amazonian rainforests, where increased sunlight leads to higher photosynthetic activity (Bi et al., 2015). Few indices, mostly water-related ones, did not show this pattern, likely because canopy water content remained high throughout the year. These findings imply that monitoring approaches must consider seasonal effects and carefully choose temporal intervals for sampling to ensure comparability among values.

With respect to combining indices for functional trait estimation, most indices within the same category had a high intercorrelation and differentiated significantly between the land-cover types. For practical monitoring, this suggests that index selection should prioritize those that exhibit meaningful temporal patterns, such as seasonality, and those that capture significant differences between land-cover types. In the case of this study this were the NDRE2, NDII and PSRI.

The analysis of functional diversity metrics revealed important findings. FRic proved highly sensitive to the mixed-pixel effects and to plot sizes that were too small relative to the

sensors spatial resolution, what is consistence with previous studies (Helfenstein et al., 2022). As a result, FRic values were too high, especially in agroforestry plots, and did not reflect ecological expectations. FDiv, in contrast, was more stable and aligned more closely with theoretical predictions and previous studies (Hauser et al., 2022). While both functional diversity metrics suffered from data gaps and noise in the time series, FDiv appeared considerably more robust than FRic under the conditions of this study. Taken together, the findings show that FDiv, in combination with a small and carefully selected set of indices, could be a promising metric for long-term monitoring in this context, whereas FRic needs some methodological adjustments.

In summary, this thesis demonstrates that satellite-derived spectral indices and functional diversity metrics hold strong promise for biodiversity monitoring in tropical regions with high cloud cover. Cloud masking effectively filled data gaps, yielding more cloud-free observations that revealed critical seasonal patterns that would otherwise be obscured. With some methodological adjustments, such as larger sample sizes and extended time series, this appears to be a promising approach for monitoring reforestation progress and functional diversity.

# 7 Outlook

This study provided first insights into the potential and limitations of satellite-based functional diversity and vegetation indices for biodiversity monitoring over different land cover types in West Kalimantan, Borneo. While the results revealed some interesting insights, they also highlight methodological constraints that need to be addressed in the future.

Future work would benefit from having denser and more regular sampling despite the high cloud coverage. The integration of other sensors such as PlanetScope data or combining multispectral imagery with radar or lidar data, could substantially improve spatial and temporal consistency. Merging data streams from multiple satellite platforms may also allow for more resilient monitoring systems that remain informative even during extended cloudy periods.

A promising direction might be the use of unmanned aerial vehicles (UAVs) that carry LiDAR or hyperspectral sensors. UAV-based remote sensing can provide higher spatial and spectral resolution and are not only able to see canopy attributes but also the understory. For example, de Almeida et al (2021) showed an approach that combined hyperspectral remote sensing and lidar with UAVs to understand changes in forest reforestation sites. Their results suggest that UAV remote sensing could play an important role in informing future reforestation policies in Borneo. Active remote-sensing technologies such as lidar or synthetic aperture radar (SAR) may improve the characterization of functional diversity by including vegetation structure. Structural metrics such as canopy height or vertical complexity might provide valuable additional information that can't be detected by optical sensors.

Several methodological aspects should also be refined in future work. Some challenges identified here were tied to the spatial characteristics of the sample-site data. Larger and more homogeneous sample-site polygons would reduce mixed-pixel effects and strengthen the interpretability of functional trait analyses. Combined with improved non-forest masking, this could considerably reduce noise in the results.

Another dimension that should be considered is how future studies could benefit from looking at how agroforestry systems might influence not only functional diversity but also

processes on landscape-scale such as connectivity. Simamora et al. (2021) have found that bird species richness declines along the land cover gradient from intact forest to monoculture plantations. However certain agroforestry systems were able to support a higher proportion of species and therefore providing meaningful conservation values. Their value was especially high when they were close to or connected to forest.

Finally, the increasing importance of transparent biodiversity monitoring in the context of sustainability reporting, deforestation-free supply chains, and international agreements highlights the relevance of further developing these approaches. With continued improvements in data availability, sensor technology, and analytical methods, satellite-based biodiversity monitoring has strong potential to support companies, land managers, and policy makers in implementing effective, scalable, and long-term monitoring strategies.

In the specific use case of Forestwise and Rahn, the results suggest a few recommendations that may support future monitoring. Because the reforestation sites are still very young, a longer time series might naturally reveal clearer trends and developments. Additionally, using larger or more uniform monitoring plots may reduce technical artefacts and strengthen the interpretation of the functional diversity metrics. With a longer time-series, satellite-based monitoring can more clearly capture the progress of Forestwise and Rahn's restoration efforts.

# Bibliograph


Addison, P.F.E., Stephenson, P.J., Bull, J.W., Carbone, G., Burgman, M., Burgass, M.J., Gerber, L.R., Howard, P., McCormick, N., McRae, L., Reuter, K.E., Starkey, M., Milner-Gulland, E.J., 2020. Bringing sustainability to life: A framework to guide biodiversity indicator development for business performance management. Bus Strat Env 29, 3303–3313. https://doi.org/10.1002/bse.2573

Affinito, F., Butchart, S.H.M., Nicholson, E., Hirsch, T., Williams, J.M., Campbell, J.E., Ferrari, M.F., Gabay, M., Gorini, L., Kalamujic Stroil, B., Kohsaka, R., Painter, B., Pinto, J.C., Scholz, A.H., Straza, T.R.A., Tshidada, N., Vallecillo, S., Widdicombe, S., Gonzalez, A., 2025. Assessing coverage of the monitoring framework of the Kunming-Montreal Global Biodiversity Framework and opportunities to fill gaps. Nat Ecol Evol 9, 1280–1294. https://doi.org/10.1038/s41559-025-02718-3

Aguirre-Gutiérrez, J., Rifai, S.W., Deng, X., Ter Steege, H., Thomson, E., Corral-Rivas, J.J., Guimaraes, A.F., Muller, S., Klipel, J., Fauset, S., Resende, A.F., Wallin, G., Joly, C.A., Abernethy, K., Adu-Bredu, S., Alexandre Silva, C., De Oliveira, E.A., Almeida, D.R.A., Alvarez-Davila, E., Asner, G.P., Baker, T.R., Benchimol, M., Bentley, L.P., Berenguer, E., Blanc, L., Bonal, D., Bordin, K., Borges De Lima, R., Both, S., Cabezas Duarte, J., Cardoso, D., De Lima, H.C., Cavalheiro, L., Cernusak, L.A., Dos Santos Prestes, N.C.C., Da Silva Zanzini, A.C., Da Silva, R.J., Dos Santos Alves Da Silva, R., De Andrade Iguatemy, M., De Sousa Oliveira, T.C., Dechant, B., Derroire, G., Dexter, K.G., Rodrigues, D.J., Espírito-Santo, M., Silva, L.F., Domingues, T.F., Ferreira, J., Simon, M.F., Girardin, C.A.J., Hérault, B., Jeffery, K.J., Kalpuzha Ashtamoorthy, S., Kavidapadinjattathil Sivadasan, A., Klitgaard, B., Laurance, W.F., Dan, M.L., Magnusson, W.E., Campos-Filho, E.M., Manoel Dos Santos, R., Manzatto, A.G., Silveira, M., Marimon-Junior, B.H., Martin, R.E., Vieira, D.L.M., Metzker, T., Milliken, W., Moonlight, P., Moraes De Seixas, M.M., Morandi, P.S., Muscarella, R., Nava-Miranda, M.G., Nyirambangutse, B., Silva, J.O., Oliveras Menor, I., Francisco Pena Rodrigues, P.J., Pereira De Oliveira, C., Pereira Zanzini, L., Peres, C.A., Punjayil, V., Quesada, C.A., Réjou-Méchain, M., Riutta, T., Rivas-Torres, G., Rosa, C., Salinas, N., Bergamin, R.S., Marimon, B.S., Shenkin, A., Silva Rodrigues, P.M., Figueiredo, A.E.S., Garcia, Q.S., Spósito, T., Storck-Tonon, D., Sullivan, M.J.P., Svátek, M., Vieira Santiago, W.T., Arn Teh, Y., Theruvil Parambil Sivan, P., Nascimento, M.T., Veenendaal, E., Zo-Bi, I.C., Dago, M.R., Traoré, S., Patacca, M., Badouard, V., De Padua Chaves E Carvalho, S., White, L.J.T., Zhang-Zheng, H., Zibera, E., Zwerts, J.A., Burslem, D.F.R.P., Silman, M., Chave, J., Enquist, B.J., Barlow, J., Phillips, O.L., Coomes, D.A., Malhi, Y., 2025. Canopy functional trait variation across Earth's tropical forests. Nature 641, 129–136. https://doi.org/10.1038/s41586-025-08663-2

Almeida, D.R.A.D., Broadbent, E.N., Ferreira, M.P., Meli, P., Zambrano, A.M.A., Gorgens, E.B., Resende, A.F., De Almeida, C.T., Do Amaral, C.H., Corte, A.P.D., Silva, C.A., Romanelli, J.P., Prata, G.A., De Almeida Papa, D., Stark, S.C., Valbuena, R., Nelson, B.W., Guillemot, J., Féret, J.-B., Chazdon, R., Brancalion, P.H.S., 2021. Monitoring restored tropical forest diversity and structure through UAV-borne hyperspectral and lidar fusion. Remote Sensing of Environment 264, 112582. https://doi.org/10.1016/j.rse.2021.112582

Asner, G.P., Martin, R.E., Suhaili, A.B., 2012. Sources of Canopy Chemical and Spectral Diversity in Lowland Bornean Forest. Ecosystems 15, 504–517. https://doi.org/10.1007/s10021-012-9526-2

Barnes, E. M., Clarke, T. R., Richards, S. E., Colaizzi, P. D., Haberland, J., Kostrzewski, M., Waller, P., Choi, C., Riley, E., Thompson, T., Lascano, R. J., Li, H., Moran, M. S., 2000. Coincident Detection of Crop Water Stress, Nitrogen Status and Canopy Density using Ground-Based Multispectral Data., in: Proceedings of the Fifth International Conference on Precision Agriculture. Bloomington, MN, USA.

Bayle, A., Carlson, B., Thierion, V., Isenmann, M., Choler, P., 2019. Improved Mapping of Mountain Shrublands Using the Sentinel-2 Red-Edge Band. Remote Sensing 11, 2807. https://doi.org/10.3390/rs11232807

Bayona, O., Ochoa, D., Criollo, R., Cevallos-Cevallos, J., Liao, W., 2018. Cocoa bean quality assessment using closed range hyperspectral images, in: 2018 Asia-Pacific Signal and Information Processing Association Annual Summit and Conference (APSIPA ASC). Presented at the 2018 Asia-Pacific Signal and Information Processing Association Annual Summit and Conference (APSIPA ASC), IEEE, Honolulu, HI, USA, pp. 622–626. https://doi.org/10.23919/APSIPA.2018.8659490

Bi, J., Knyazikhin, Y., Choi, S., Park, T., Barichivich, J., Ciais, P., Fu, R., Ganguly, S., Hall, F., Hilker, T., Huete, A., Jones, M., Kimball, J., Lyapustin, A.I., Mõttus, M., Nemani, R.R., Piao, S., Poulter, B., Saleska, S.R., Saatchi, S.S., Xu, L., Zhou, L., Myneni, R.B., 2015. Sunlight mediated seasonality in canopy structure and photosynthetic activity of Amazonian rainforests. Environ. Res. Lett. 10, 064014. https://doi.org/10.1088/1748-9326/10/6/064014

Bourgoin, C., Verhegghen, A., Degreve, L., Ameztoy, I., Carboni, S., Colditz, R., Achard, F., 2024. Global map of forest cover 2020 - version 2.

Butchart, S.H.M., Miloslavich de Klein, P., Reyers, B., Subramanian, S.M., Adams, C., Bennett, E., Czúcz, B., Galetto, L., Galvin, K., Reyes-García, V., Gerber, L.R., Gode, T.B., Jetz, W., Mphangwe Kosamu, I.B.M.K., Palomo, M.G., Panahi, M., Selig, E.R., Singh, G.S., Tarkhnishvili, D., Xu, H., Lynch, A.J., Mwampamba, T.H., Samakov, A., 2019. Chapter 3. Assessing progress towards meeting major international objectives related to nature and nature's contributions to people. Zenodo. https://doi.org/10.5281/ZENODO.3832053

Cavalaris, C., Megoudi, S., Maxouri, M., Anatolitis, K., Sifakis, M., Levizou, E., Kyparissis, A., 2021. Modeling of Durum Wheat Yield Based on Sentinel-2 Imagery. Agronomy 11, 1486. https://doi.org/10.3390/agronomy11081486

Cheng, Y.-B., Ustin, S.L., Riaño, D., Vanderbilt, V.C., 2008. Water content estimation from hyperspectral images and MODIS indexes in Southeastern Arizona. Remote Sensing of Environment 112, 363–374. https://doi.org/10.1016/j.rse.2007.01.023

Cheng, Y.-B., Zarco-Tejada, P.J., Riaño, D., Rueda, C.A., Ustin, S.L., 2006. Estimating vegetation water content with hyperspectral data for different canopy scenarios: Relationships between AVIRIS and MODIS indexes. Remote Sensing of Environment 105, 354–366. https://doi.org/10.1016/j.rse.2006.07.005

Çinar, T., Uslu, A., Aydin, A., 2025. Monitoring the rehabilitation process of the windthrow area using UAS images and performance comparison of Sentinel-2A based different vegetation indexes. Earth Sci Inform 18, 199. https://doi.org/10.1007/s12145-025-01701-7

Clevers, J.G.P.W., Gitelson, A.A., 2013. Remote estimation of crop and grass chlorophyll and nitrogen content using red-edge bands on Sentinel-2 and -3. International Journal of Applied Earth Observation and Geoinformation 23, 344–351. https://doi.org/10.1016/j.jag.2012.10.008

Cohen, T.A., Brook, A., Zbedat, G., 2024. Long-Term Land Restoration Assessment Using Remote Sensing in Mediterranean Ecosystems, in: 2024 IEEE International Workshop on Metrology for Agriculture and Forestry (MetroAgriFor). Presented at the 2024 IEEE International Workshop on Metrology for Agriculture and Forestry (MetroAgriFor), IEEE, Padua, Italy, pp. 179–183. https://doi.org/10.1109/MetroAgriFor63043.2024.10948855

Colombo, R., Meroni, M., Marchesi, A., Busetto, L., Rossini, M., Giardino, C., Panigada, C., 2008. Estimation of leaf and canopy water content in poplar plantations by means of hyperspectral indices and inverse modeling. Remote Sensing of Environment 112, 1820–1834. https://doi.org/10.1016/j.rse.2007.09.005

Convention on Biological Diversity (COP), 2010. Decision adopted by the Conference of the Parties to the Convention on Biological Diversity at its Tenth Meeting: X/2. The Strategic Plan for Biodiversity 2011–2020 and the Aichi Biodiversity Targets (COP Decision). Secretariat of the Convention on Biological Diversity, Nagoya, Japan.

Cui, B., Zhao, Q., Huang, W., Song, X., Ye, H., Zhou, X., 2019. Leaf chlorophyll content retrieval of wheat by simulated RapidEye, Sentinel-2 and EnMAP data. Journal of Integrative Agriculture 18, 1230–1245. https://doi.org/10.1016/S2095-3119(18)62093-3

Dash, J., Curran, P.J., 2004. The MERIS terrestrial chlorophyll index. International Journal of Remote Sensing 25, 5403–5413. https://doi.org/10.1080/0143116042000274015

Dash, J., Jeganathan, C., Atkinson, P.M., 2010. The use of MERIS Terrestrial Chlorophyll Index to study spatio-temporal variation in vegetation phenology over India. Remote Sensing of Environment 114, 1388–1402. https://doi.org/10.1016/j.rse.2010.01.021

Daughtry, C.S.T., Walthall, C.L, Kim, M.S, Brown de Colstoun, E., McMurtrey III, J.E, 2000. Estimating Corn Leaf Chlorophyll Concentration from Leaf and Canopy Reflectance. Remote Sensing of Environment 74, 229–239. https://doi.org/10.1016/S0034-4257(00)00113-9

Descals, A., Wich, S., Meijaard, E., Gaveau, D.L.A., Peedell, S., Szantoi, Z., 2021a. High resolution global industrial and smallholder oil palm map for 2019. https://doi.org/10.5281/ZENODO.3884601

Descals, A., Wich, S., Meijaard, E., Gaveau, D.L.A., Peedell, S., Szantoi, Z., 2021b. High-resolution global map of smallholder and industrial closed-canopy oil palm plantations. Earth Syst. Sci. Data 13, 1211–1231. https://doi.org/10.5194/essd-13-1211-2021

Díaz, S., Fargione, J., Chapin, F.S., Tilman, D., 2006. Biodiversity Loss Threatens Human Well-Being. PLoS Biol 4, e277. https://doi.org/10.1371/journal.pbio.0040277

Dotzler, S., Hill, J., Buddenbaum, H., Stoffels, J., 2015. The Potential of EnMAP and Sentinel-2 Data for Detecting Drought Stress Phenomena in Deciduous Forest Communities. Remote Sensing 7, 14227–14258. https://doi.org/10.3390/rs71014227

Duffy, C., Toth, G.G., Hagan, R.P.O., McKeown, P.C., Rahman, S.A., Widyaningsih, Y., Sunderland, T.C.H., Spillane, C., 2021. Agroforestry contributions to smallholder farmer food security in Indonesia. Agroforest Syst 95, 1109–1124. https://doi.org/10.1007/s10457-021-00632-8

European Commission. Joint Research Centre., Bourgoin, C., Ameztoy, I., Verhegghen, A., Desclée, B., Carboni, S., Bastin, J., Beuchle, R., Brink, A., Defourny, P., Delhez, B., Fritz, S., Gond, V., Herold, M., Lamarche, C., Mansuy, N., Mollicone, D., Oom, D., Peedell, S., San-Miguel, J., Colditz, R., Achard, F., 2024. Mapping global forest cover of the year 2020 to support the EU regulation on deforestation-free supply chains. Publications Office of the European Union, Luxembourg.

European Space Agency, 2022. Sentinel-2 MSI Level-2A BOA Reflectance. https://doi.org/10.5270/S2_-znk9xsj

Fan, Y., Meijide, A., Lawrence, D.M., Roupsard, O., Carlson, K.M., Chen, H., Röll, A., Niu, F., Knohl, A., 2019. Reconciling Canopy Interception Parameterization and Rainfall Forcing Frequency in the Community Land Model for Simulating Evapotranspiration of Rainforests and Oil Palm Plantations in Indonesia. J Adv Model Earth Syst 11, 732–751. https://doi.org/10.1029/2018MS001490

Ferreira, M.B., Ferreira, R.L.C., Da Silva, J.A.A., De Lima, R.B., Silva, E.A., De Sousa, A.N., De La Cruz, D.B.C., Da Silva, M.V., 2024. Spatial-Temporal Dynamics of Water Resources in Seasonally Dry Tropical Forest: Causes and Vegetation Response. AgriEngineering 6, 2526–2552. https://doi.org/10.3390/agriengineering6030148

Ferreira, M.P., Féret, J.-B., Grau, E., Gastellu-Etchegorry, J.-P., Do Amaral, C.H., Shimabukuro, Y.E., De Souza Filho, C.R., 2018. Retrieving structural and chemical properties of individual tree crowns in a highly diverse tropical forest with 3D radiative transfer modeling and imaging spectroscopy. Remote Sensing of Environment 211, 276–291. https://doi.org/10.1016/j.rse.2018.04.023

Food and Agriculture Organization, 2018. Global Forest Resources Assessment 2020 - Terms and Definitions. (No. Forest Resources Assessment Working Paper 188,). Rome.

Fowler, D., Nemitz, E., Misztal, P., Di Marco, C., Skiba, U., Ryder, J., Helfter, C., Cape, J.N., Owen, S., Dorsey, J., Gallagher, M.W., Coyle, M., Phillips, G., Davison, B., Langford, B., MacKenzie, R., Muller, J., Siong, J., Dari-Salisburgo, C., Di Carlo, P., Aruffo, E., Giammaria, F., Pyle, J.A., Hewitt, C.N., 2011. Effects of land use on surface–atmosphere exchanges of trace gases and energy in Borneo: comparing fluxes over oil palm plantations and a rainforest. Phil. Trans. R. Soc. B 366, 3196–3209. https://doi.org/10.1098/rstb.2011.0055

Gao, B., 1996. NDWI—A normalized difference water index for remote sensing of vegetation liquid water from space. Remote Sensing of Environment 58, 257–266. https://doi.org/10.1016/S0034-4257(96)00067-3

Gaveau, D.L.A., Locatelli, B., Salim, M.A., Yaen, H., Pacheco, P., Sheil, D., 2018. Rise and fall of forest loss and industrial plantations in Borneo (2000–2017). CONSERVATION LETTERS 12, e12622. https://doi.org/10.1111/conl.12622

Gillies, S., van der Wel, C., Van den Bossche, J., Taves, M.W., Arnott, J., Ward, B.C., others, 2025. Shapely. https://doi.org/10.5281/ZENODO.5597138

Gitelson, A., Merzlyak, M.N., 1994. Quantitative estimation of chlorophyll-a using reflectance spectra: Experiments with autumn chestnut and maple leaves. Journal of Photochemistry and Photobiology B: Biology 22, 247–252. https://doi.org/10.1016/1011-1344(93)06963-4

Gitelson, A.A., Chivkunova, O.B., Merzlyak, M.N., 2009. Nondestructive estimation of anthocyanins and chlorophylls in anthocyanic leaves. American J of Botany 96, 1861–1868. https://doi.org/10.3732/ajb.0800395

Gitelson, A.A., Keydan, G.P., Merzlyak, M.N., 2006. Three-band model for noninvasive estimation of chlorophyll, carotenoids, and anthocyanin contents in higher plant leaves. Geophysical Research Letters 33, 2006GL026457. https://doi.org/10.1029/2006GL026457

Gitelson, A.A., Merzlyak, M.N., Chivkunova, O.B., 2001. Optical Properties and Nondestructive Estimation of Anthocyanin Content in Plant Leaves. Photochem Photobiol 74, 38. https://doi.org/10.1562/0031-8655(2001)074%253C0038:OPANEO%253E2.0.CO;2

Gitelson, A.A., Zur, Y., Chivkunova, O.B., Merzlyak, M.N., 2007. Assessing Carotenoid Content in Plant Leaves with Reflectance Spectroscopy¶. Photochemistry and Photobiology 75, 272–281. https://doi.org/10.1562/0031-8655(2002)0750272ACCIPL2.0.CO2

Gorelick, N., Hancher, M., Dixon, M., Ilyushchenko, S., Thau, D., Moore, R., 2017. Google Earth Engine: Planetary-scale geospatial analysis for everyone. Remote Sensing of Environment 202, 18–27. https://doi.org/10.1016/j.rse.2017.06.031

Gupta, S.K., Pandey, A.C., 2021. Spectral aspects for monitoring forest health in extreme season using multispectral imagery. The Egyptian Journal of Remote Sensing and Space Science 24, 579–586. https://doi.org/10.1016/j.ejrs.2021.07.001

Haboudane, D., Miller, J.R., Tremblay, N., Zarco-Tejada, P.J., Dextraze, L., 2002. Integrated narrow-band vegetation indices for prediction of crop chlorophyll content for application to precision agriculture. Remote Sensing of Environment 81, 416–426. https://doi.org/10.1016/S0034-4257(02)00018-4

Hardisky, M.A., Michael Smart, R., Klemas, V., 1983. Growth response and spectral characteristics of a short Spartina alterniflora salt marsh irrigated with freshwater and sewage effluent. Remote Sensing of Environment 13, 57–67. https://doi.org/10.1016/0034-4257(83)90027-5

Harris, C.R., Millman, K.J., Van Der Walt, S.J., Gommers, R., Virtanen, P., Cournapeau, D., Wieser, E., Taylor, J., Berg, S., Smith, N.J., Kern, R., Picus, M., Hoyer, S., Van Kerkwijk, M.H., Brett, M., Haldane, A., Del Río, J.F., Wiebe, M., Peterson, P., Gérard-Marchant, P., Sheppard, K., Reddy, T., Weckesser, W., Abbasi, H., Gohlke, C., Oliphant, T.E., 2020. Array programming with NumPy. Nature 585, 357–362. https://doi.org/10.1038/s41586-020-2649-2

Hashimoto, H., Uragami, C., Cogdell, R.J., 2016. Carotenoids and Photosynthesis, in: Stange, C. (Ed.), Carotenoids in Nature, Subcellular Biochemistry. Springer International Publishing, Cham, pp. 111–139. https://doi.org/10.1007/978-3-319-39126-7_4

Hauser, L.T., Timmermans, J., Soudzilovskaia, N.A., Van Bodegom, P.M., 2022. Linking Land Use and Plant Functional Diversity Patterns in Sabah, Borneo, through Large-Scale Spatially Continuous Sentinel-2 Inference. Land 11, 572. https://doi.org/10.3390/land11040572

Helfenstein, I., 2024. Towards Monitoring Biodiversity from Space. University of Zurich, Mathematisch-naturwissenschaftliche Fakultät. https://doi.org/10.5167/UZH-264328

Helfenstein, I.S., Schneider, F.D., Schaepman, M.E., Morsdorf, F., 2022. Assessing biodiversity from space: Impact of spatial and spectral resolution on trait-based functional diversity. Remote Sensing of Environment 275, 113024. https://doi.org/10.1016/j.rse.2022.113024

Huang, J., Wei, Chen, Zhang, Y., Blackburn, G.A., Wang, X., Wei, Chuanwen, Wang, J., 2015. Meta-Analysis of the Detection of Plant Pigment Concentrations Using Hyperspectral

Remotely Sensed Data. PLoS ONE 10, e0137029. https://doi.org/10.1371/journal.pone.0137029

Huete, A., Didan, K., Miura, T., Rodriguez, E.P., Gao, X., Ferreira, L.G., 2002. Overview of the radiometric and biophysical performance of the MODIS vegetation indices. Remote Sensing of Environment 83, 195–213. https://doi.org/10.1016/S0034-4257(02)00096-2

Hunt, E.R., Rock, B.N., 1989. Detection of changes in leaf water content using Near- and Middle-Infrared reflectances☆. Remote Sensing of Environment 30, 43–54. https://doi.org/10.1016/0034-4257(89)90046-1

Ievinsh, G., 2023. Water Content of Plant Tissues: So Simple That Almost Forgotten? Plants 12, 1238. https://doi.org/10.3390/plants12061238

Jetz, W., Cavender-Bares, J., Pavlick, R., Schimel, D., Davis, F.W., Asner, G.P., Guralnick, R., Kattge, J., Latimer, A.M., Moorcroft, P., Schaepman, M.E., Schildhauer, M.P., Schneider, F.D., Schrodt, F., Stahl, U., Ustin, S.L., 2016. Monitoring plant functional diversity from space. Nature Plants 2, 16024. https://doi.org/10.1038/nplants.2016.24

Kanu, B., Parida, B.R., Bar, S., Dwivedi, C.S., Pandey, A.C., 2025. Estimating forest biophysical and biochemical parameters in Behali Reserve Forest (Assam) using proximal and remote sensing techniques. Trop Ecol 66, 1–13. https://doi.org/10.1007/s42965-024-00359-4

Khokthong, W., Zemp, D.C., Irawan, B., Sundawati, L., Kreft, H., Hölscher, D., 2019. Drone-Based Assessment of Canopy Cover for Analyzing Tree Mortality in an Oil Palm Agroforest. Front. For. Glob. Change 2, 12. https://doi.org/10.3389/ffgc.2019.00012

Kior, A., Sukhov, V., Sukhova, E., 2021. Application of Reflectance Indices for Remote Sensing of Plants and Revealing Actions of Stressors. Photonics 8, 582. https://doi.org/10.3390/photonics8120582

Korhonen, L., Hadi, Packalen, P., Rautiainen, M., 2017a. Comparison of Sentinel-2 and Landsat 8 in the estimation of boreal forest canopy cover and leaf area index. Remote Sensing of Environment 195, 259–274. https://doi.org/10.1016/j.rse.2017.03.021

Korhonen, L., Hadi, Packalen, P., Rautiainen, M., 2017b. Comparison of Sentinel-2 and Landsat 8 in the estimation of boreal forest canopy cover and leaf area index. Remote Sensing of Environment 195, 259–274. https://doi.org/10.1016/j.rse.2017.03.021

Kriegler, F.J., 1969. Preprocessing transformations and their effects on multspectral recognition, in: Proceedings of the Sixth International Symposium on Remote Sensing of Environment. pp. 97–131.

Le Minh Hang, B.X.H., Nga, N.T., Pham, M.P., Khanh, N.Q., 2024. Evaluation of Cloud Masking Methods using Sentinel-2 Satellite Images on Google Earth Engine: A Case Study in Vietnam. Int. J. Econ. Environ. Geol. 15, 26–33.

Lee, J.H., Kwon, Y.B., Roh, Y.H., Choi, I.-L., Kim, J., Kim, Y., Yoon, H.S., Kang, H.-M., 2023. Effect of Various LED Light Qualities, Including Wide Red Spectrum-LED, on the Growth and Quality of Mini Red Romaine Lettuce (cv. Breen). Plants 12, 2056. https://doi.org/10.3390/plants12102056

Leonald, L., Rowland, D., 2016. Drivers and effects of agrarian change in Kapuas Hulu Regency, West Kalimantan, Indonesia, in: Agrarian Change in Tropical Landscapes. Center for International Forestry Research (CIFOR), Bogor, Indonesia.

Li, Z., Ahammed, G.J., 2023. Plant stress response and adaptation via anthocyanins: A review. Plant Stress 10, 100230. https://doi.org/10.1016/j.stress.2023.100230

Lindenmayer, D.B., Gibbons, P., Bourke, M., Burgman, M., Dickman, C.R., Ferrier, S., Fitzsimons, J., Freudenberger, D., Garnett, S.T., Groves, C., Hobbs, R.J., Kingsford, R.T.,

Krebs, C., Legge, S., Lowe, A.J., Mclean, R., Montambault, J., Possingham, H., Radford, J., Robinson, D., Smallbone, L., Thomas, D., Varcoe, T., Vardon, M., Wardle, G., Woinarski, J., Zerger, A., 2011. Improving biodiversity monitoring. Austral Ecology 37, 285–294. https://doi.org/10.1111/j.1442-9993.2011.02314.x

Mansur, M., Brearley, F.Q., 2023. Biomass and floristics of a secondary forest in West Kalimantan, Indonesia. Tropics 32, 85–93. https://doi.org/10.3759/tropics.MS22-09

Mason, N.W.H., Mouillot, D., Lee, W.G., Wilson, J.B., 2005. Functional richness, functional evenness and functional divergence: the primary components of functional diversity. Oikos 111, 112–118. https://doi.org/10.1111/j.0030-1299.2005.13886.x

Mathys, A.S., Van Vianen, J., Rowland, D., Narulita, S., Palomo, I., Pascual, U., Sutherland, I.J., Ahammad, R., Sunderland, T., 2023. Participatory mapping of ecosystem services across a gradient of agricultural intensification in West Kalimantan, Indonesia. Ecosystems and People 19, 2174685. https://doi.org/10.1080/26395916.2023.2174685

McLachlan, G.J., 1999. Mahalanobis distance. Reson 4, 20–26. https://doi.org/10.1007/BF02834632

Mederer, D., Kattenborn, T., Cherif, E., Guimaraes-Steinicke, C., Joswig, J.S., Schneider, F.D., Feilhauer, H., 2025. Unraveling the seasonality of functional diversity through remote sensing. Commun Earth Environ 6, 790. https://doi.org/10.1038/s43247-025-02646-x

Merzlyak, M.N., Gitelson, A.A., Chivkunova, O.B., Rakitin, V.Yu., 1999. Non-destructive optical detection of pigment changes during leaf senescence and fruit ripening. Physiologia Plantarum 106, 135–141. https://doi.org/10.1034/j.1399-3054.1999.106119.x

Mielke, M.S., Schaffer, B., Schilling, A.C., 2012. Evaluation of reflectance spectroscopy indices for estimation of chlorophyll content in leaves of a tropical tree species. Photosynt. 50, 343–352. https://doi.org/10.1007/s11099-012-0038-2

Mirzaie, M., Darvishzadeh, R., Shakiba, A., Matkan, A.A., Atzberger, C., Skidmore, A., 2014. Comparative analysis of different uni- and multi-variate methods for estimation of vegetation water content using hyper-spectral measurements. International Journal of Applied Earth Observation and Geoinformation 26, 1–11. https://doi.org/10.1016/j.jag.2013.04.004

Montes-Bojórquez, M.G., Robles-Zazueta, C.A., Tinoco-Ojanguren, C., Enquist, B.J., Frazier, A.E., Maitner, B.S., Moulatlet, G.M., Romo-León, J.R., Song, L., Hinojo-Hinojo, C., 2025. Challenges and opportunities in detecting leaf water and carotenoid content across biomes from satellite multispectral indices. https://doi.org/10.1101/2025.11.01.686024

Murphy, D.J., 2024. Carbon Sequestration by Tropical Trees and Crops: A Case Study of Oil Palm. Agriculture 14, 1133. https://doi.org/10.3390/agriculture14071133

Murphy, D.J., Goggin, K., Paterson, R.R.M., 2021. Oil palm in the 2020s and beyond: challenges and solutions. CABI Agric Biosci 2, 39. https://doi.org/10.1186/s43170-021-00058-3

Nair, P.K.R., Kumar, B.M., Nair, V.D., 2021. An Introduction to Agroforestry: Four Decades of Scientific Developments, Second Edition. ed. Springer International Publishing, Cham. https://doi.org/10.1007/978-3-030-75358-0

Nunes, M.H., Both, S., Bongalov, B., Brelsford, C., Khoury, S., Burslem, D.F.R.P., Philipson, C., Majalap, N., Riutta, T., Coomes, D.A., Cutler, M.E.J., 2019. Changes in leaf functional traits of rainforest canopy trees associated with an El Niño event in Borneo. Environ. Res. Lett. 14, 085005. https://doi.org/10.1088/1748-9326/ab2eae

Oliveira Santos, R.D., Delgado, R.C., Vilanova, R.S., Santana, R.O.D., Andrade, C.F.D., Teodoro, P.E., Silva Junior, C.A., Capristo-Silva, G.F., Lima, M., 2021. NMDI application for monitoring different vegetation covers in the Atlantic Forest biome,

Brazil. Weather and Climate Extremes 33, 100329. https://doi.org/10.1016/j.wace.2021.100329

Otsu, N., 1979. A Threshold Selection Method from Gray-Level Histograms. IEEE Trans. Syst., Man, Cybern. 9, 62–66. https://doi.org/10.1109/TSMC.1979.4310076

Padalia, H., Sinha, S.K., Bhave, V., Trivedi, N.K., Senthil Kumar, A., 2020. Estimating canopy LAI and chlorophyll of tropical forest plantation (North India) using Sentinel-2 data. Advances in Space Research 65, 458–469. https://doi.org/10.1016/j.asr.2019.09.023

Pansit, N.R., Parilla, R.B., 2024. Detecting Vegetation Cover Change in Reforestation Sites from 2013 to 2019 in Central Visayas, Philippines Using Remotely Sensed Data. MJST 22. https://doi.org/10.61310/mjst.v22i1.1961

Papes, M., Tupayachi, R., Martinez, P., Peterson, A.T., Asner, G.P., Powell, G.V.N., 2013. Seasonal Variation in Spectral Signatures of Five Genera of Rainforest Trees. IEEE J. Sel. Top. Appl. Earth Observations Remote Sensing 6, 339–350. https://doi.org/10.1109/JSTARS.2012.2228468

Pasqualotto, N., Delegido, J., Van Wittenberghe, S., Rinaldi, M., Moreno, J., 2019. Multi-Crop Green LAI Estimation with a New Simple Sentinel-2 LAI Index (SeLI). Sensors 19, 904. https://doi.org/10.3390/s19040904

Pasquarella, V.J., Brown, C.F., Czerwinski, W., Rucklidge, W.J., 2023. Comprehensive quality assessment of optical satellite imagery using weakly supervised video learning, in: 2023 IEEE/CVF Conference on Computer Vision and Pattern Recognition Workshops (CVPRW). Presented at the 2023 IEEE/CVF Conference on Computer Vision and Pattern Recognition Workshops (CVPRW), IEEE, Vancouver, BC, Canada, pp. 2125–2135. https://doi.org/10.1109/CVPRW59228.2023.00206

Petchey, O.L., Gaston, K.J., 2002. Functional diversity (FD), species richness and community composition. Ecology Letters 5, 402–411. https://doi.org/10.1046/j.1461-0248.2002.00339.x

Planet Labs PBC, 2025. Planet Application Program Interface: In Space for Life on Earth.

Pribadi, U.A., Setiabudy, Suryadi, I., Laumonier, Y., 2020. West Kalimantan Ecological Vegetation Map 1:50 000. https://doi.org/10.17528/CIFOR/DATA.00203

QGIS Development Team, 2025. QGIS Geographic Information System.

Rao, A.S., Chhawri, R., Chauhan, A., Yadav, S.S., Meena, K.C., Bansal, P., 2024. Plant Functional Traits: A Key Framework for Understanding and Managing Ecosystem Responses to Global Environmental Challenges, in: Kumar, N., Singh, H. (Eds.), Plant Functional Traits for Improving Productivity. Springer Nature Singapore, Singapore, pp. 287–299. https://doi.org/10.1007/978-981-97-1510-7_15

Restor Foundation, 2024. Restor [WWW Document]. Willkommen bei Restor. URL https://restor.eco/de/?lat=25.534247489073934&lng=14.379981694202483&zoom=3.087626763916016 (accessed 4.27.25).

Rhodes, C.J., Henrys, P., Siriwardena, G.M., Whittingham, M.J., Norton, L.R., 2015. The relative value of field survey and remote sensing for biodiversity assessment. Methods Ecol Evol 6, 772–781. https://doi.org/10.1111/2041-210X.12385

Rondeaux, G., Steven, M., Baret, F., 1996. Optimization of soil-adjusted vegetation indices. Remote Sensing of Environment 55, 95–107. https://doi.org/10.1016/0034-4257(95)00186-7

Rubilar, R.A., Valverde, J.C., Barrientos, G., Campoe, O.C., 2024. Water and Temperature Ecophysiological Challenges of Forests Plantations under Climate Change. Forests 15, 654. https://doi.org/10.3390/f15040654

Sa'adi, Z., Shahid, S., Shiru, M.S., 2021. Defining climate zone of Borneo based on cluster analysis. Theor Appl Climatol 145, 1467–1484. https://doi.org/10.1007/s00704-021-03701-1

Schneider, F.D., Morsdorf, F., Schmid, B., Petchey, O.L., Hueni, A., Schimel, D.S., Schaepman, M.E., 2017. Mapping functional diversity from remotely sensed morphological and physiological forest traits. Nat Commun 8, 1441. https://doi.org/10.1038/s41467-017-01530-3

Simamora, T.I., Purbowo, S.D., Laumonier, Y., 2021. Looking for indicator bird species in the context of forest fragmentation and isolation in West Kalimantan, Indonesia. Global Ecology and Conservation 27, e01610. https://doi.org/10.1016/j.gecco.2021.e01610

Sims, D.A., Gamon, J.A., 2003. Estimation of vegetation water content and photosynthetic tissue area from spectral reflectance: a comparison of indices based on liquid water and chlorophyll absorption features. Remote Sensing of Environment 84, 526–537. https://doi.org/10.1016/S0034-4257(02)00151-7

Son, N.-T., Chen, C.-F., Chen, C.-R., Guo, H.-Y., 2020. Classification of multitemporal Sentinel-2 data for field-level monitoring of rice cropping practices in Taiwan. Advances in Space Research 65, 1910–1921. https://doi.org/10.1016/j.asr.2020.01.028

Stephenson, P.J., Londoño-Murcia, M.C., Borges, P.A.V., Claassens, L., Frisch-Nwakanma, H., Ling, N., McMullan-Fisher, S., Meeuwig, J.J., Unter, K.M.M., Walls, J.L., Burfield, I.J., Do Carmo Vieira Correa, D., Geller, G.N., Montenegro Paredes, I., Mubalama, L.K., Ntiamoa-Baidu, Y., Roesler, I., Rovero, F., Sharma, Y.P., Wiwardhana, N.W., Yang, J., Fumagalli, L., 2022. Measuring the Impact of Conservation: The Growing Importance of Monitoring Fauna, Flora and Funga. Diversity 14, 824. https://doi.org/10.3390/d14100824

Talebzadeh, F., Valeo, C., 2022. Evaluating the Effects of Environmental Stress on Leaf Chlorophyll Content as an Index for Tree Health. IOP Conf. Ser.: Earth Environ. Sci. 1006, 012007. https://doi.org/10.1088/1755-1315/1006/1/012007

The Matplotlib Development Team, 2024. Matplotlib: Visualization with Python. https://doi.org/10.5281/ZENODO.14464227

The pandas development team, 2024. pandas-dev/pandas: Pandas. https://doi.org/10.5281/ZENODO.13819579

Tyagi, J., Kumar, M., 2024. Plant Functional Trait: Concept and Significance, in: Kumar, N., Singh, H. (Eds.), Plant Functional Traits for Improving Productivity. Springer Nature Singapore, Singapore, pp. 1–22. https://doi.org/10.1007/978-981-97-1510-7_1

Van den Bossche, J., Jordahl, K., Fleischmann, M., Richards, M., McBride, J., Wasserman, J., Garcia Badaracco, A., Snow, A.D., Ward, B., Tratner, J., Gerard, J., Perry, M., cjqf, Hjelle, G., Taves, M., ter Hoeven, E., Cochran, M., Bell, R., rraymondgh, Bartos, M., Roggemans, P., Culbertson, L., Caria, G., Tan, N., Eubank, N., sangarshanan, Flavin, J., Rey, S., Gardiner, J., 2024. geopandas/geopandas: v1.0.1. https://doi.org/10.5281/ZENODO.12625316

Van Passel, J., De Keersmaecker, W., Somers, B., 2020. Monitoring Woody Cover Dynamics in Tropical Dry Forest Ecosystems Using Sentinel-2 Satellite Imagery. Remote Sensing 12, 1276. https://doi.org/10.3390/rs12081276

Varghese, D., Radulović, M., Stojković, S., Crnojević, V., 2021. Reviewing the Potential of Sentinel-2 in Assessing the Drought. Remote Sensing 13, 3355. https://doi.org/10.3390/rs13173355

Vijith, H., Dodge-Wan, D., 2020. Applicability of MODIS land cover and Enhanced Vegetation Index (EVI) for the assessment of spatial and temporal changes in strength of vegetation in tropical rainforest region of Borneo. Remote Sensing Applications: Society and Environment 18, 100311. https://doi.org/10.1016/j.rsase.2020.100311

Virtanen, P., Gommers, R., Oliphant, T.E., Haberland, M., Reddy, T., Cournapeau, D., Burovski, E., Peterson, P., Weckesser, W., Bright, J., Van Der Walt, S.J., Brett, M., Wilson, J., Millman, K.J., Mayorov, N., Nelson, A.R.J., Jones, E., Kern, R., Larson, E., Carey, C.J., Polat, İ., Feng, Y., Moore, E.W., VanderPlas, J., Laxalde, D., Perktold, J., Cimrman, R., Henriksen, I., Quintero, E.A., Harris, C.R., Archibald, A.M., Ribeiro, A.H., Pedregosa, F., Van Mulbregt, P., SciPy 1.0 Contributors, Vijaykumar, A., Bardelli, A.P., Rothberg, A., Hilboll, A., Kloeckner, A., Scopatz, A., Lee, A., Rokem, A., Woods, C.N., Fulton, C., Masson, C., Häggström, C., Fitzgerald, C., Nicholson, D.A., Hagen, D.R., Pasechnik, D.V., Olivetti, E., Martin, E., Wieser, E., Silva, F., Lenders, F., Wilhelm, F., Young, G., Price, G.A., Ingold, G.-L., Allen, G.E., Lee, G.R., Audren, H., Probst, I., Dietrich, J.P., Silterra, J., Webber, J.T., Slavič, J., Nothman, J., Buchner, J., Kulick, J., Schönberger, J.L., De Miranda Cardoso, J.V., Reimer, J., Harrington, J., Rodríguez, J.L.C., Nunez-Iglesias, J., Kuczynski, J., Tritz, K., Thoma, M., Newville, M., Kümmerer, M., Bolingbroke, M., Tartre, M., Pak, M., Smith, N.J., Nowaczyk, N., Shebanov, N., Pavlyk, O., Brodtkorb, P.A., Lee, P., McGibbon, R.T., Feldbauer, R., Lewis, S., Tygier, S., Sievert, S., Vigna, S., Peterson, S., More, S., Pudlik, T., Oshima, T., Pingel, T.J., Robitaille, T.P., Spura, T., Jones, T.R., Cera, T., Leslie, T., Zito, T., Krauss, T., Upadhyay, U., Halchenko, Y.O., Vázquez-Baeza, Y., 2020. SciPy 1.0: fundamental algorithms for scientific computing in Python. Nat Methods 17, 261–272. https://doi.org/10.1038/s41592-019-0686-2

Wang, J., Xu, R., Yang, S., 2009. Estimation of plant water content by spectral absorption features centered at 1,450 nm and 1,940 nm regions. Environ Monit Assess 157, 459–469. https://doi.org/10.1007/s10661-008-0548-3

Wang, L., Qu, J.J., 2007. NMDI: A normalized multi-band drought index for monitoring soil and vegetation moisture with satellite remote sensing. Geophysical Research Letters 34, 2007GL031021. https://doi.org/10.1029/2007GL031021

Wang, X., Cai, G., Lu, X., Yang, Z., Zhang, X., Zhang, Q., 2022. Inversion of Wheat Leaf Area Index by Multivariate Red-Edge Spectral Vegetation Index. Sustainability 14, 15875. https://doi.org/10.3390/su142315875

Wani, A.A., Bhat, A.F., Gatoo, A.A., Zahoor, S., Mehraj, B., Najam, N., Wani, Q.S., Islam, M.A., Murtaza, S., Dervash, M.A., Joshi, P.K., 2021. Assessing relationship of forest biophysical factors with NDVI for carbon management in key coniferous strata of temperate Himalayas. Mitig Adapt Strateg Glob Change 26, 1. https://doi.org/10.1007/s11027-021-09937-6

Waskom, M., 2021. seaborn: statistical data visualization. JOSS 6, 3021. https://doi.org/10.21105/joss.03021

Wu, Q., 2020. geemap: A Python package for interactive mapping with Google Earth Engine. JOSS 5, 2305. https://doi.org/10.21105/joss.02305

Yilmaz, M.T., Hunt, E.R., Goins, L.D., Ustin, S.L., Vanderbilt, V.C., Jackson, T.J., 2008. Vegetation water content during SMEX04 from ground data and Landsat 5 Thematic Mapper imagery. Remote Sensing of Environment 112, 350–362. https://doi.org/10.1016/j.rse.2007.03.029

Zarco-Tejada, P.J., Hornero, A., Beck, P.S.A., Kattenborn, T., Kempeneers, P., Hernández-Clemente, R., 2019. Chlorophyll content estimation in an open-canopy conifer forest

with Sentinel-2A and hyperspectral imagery in the context of forest decline. Remote Sensing of Environment 223, 320–335. https://doi.org/10.1016/j.rse.2019.01.031

Zhao, X., Zhang, Y., Long, T., Wang, S., Yang, J., 2022. Regulation Mechanism of Plant Pigments Biosynthesis: Anthocyanins, Carotenoids, and Betalains. Metabolites 12, 871. https://doi.org/10.3390/metabo12090871

Zhao, Y., Potgieter, A.B., Zhang, M., Wu, B., Hammer, G.L., 2020. Predicting Wheat Yield at the Field Scale by Combining High-Resolution Sentinel-2 Satellite Imagery and Crop Modelling. Remote Sensing 12, 1024. https://doi.org/10.3390/rs12061024

Zheng, Z., Schmid, B., Zeng, Y., Schuman, M.C., Zhao, D., Schaepman, M.E., Morsdorf, F., 2023. Remotely sensed functional diversity and its association with productivity in a subtropical forest. Remote Sensing of Environment 290, 113530. https://doi.org/10.1016/j.rse.2023.113530

Zhou, H., Zhou, G., Song, X., He, Q., 2022. Dynamic Characteristics of Canopy and Vegetation Water Content during an Entire Maize Growing Season in Relation to Spectral-Based Indices. Remote Sensing 14, 584. https://doi.org/10.3390/rs14030584

# Personal Declaration

I hereby declare that the submitted thesis is the result of my own, independent work. All external sources are explicitly acknowledged in the thesis.

Date, Place

30. 11. 2025, Will SG

Signature

N. Nitsingam

Nathalie Nitsingam

# Disclosure Statement for the use of AI

AI was used for this work, namely: ChatGPT-4, ChatGPT-5, Perplexity, Deepl, Consensus.
I used AI for the following purposes:

1. To edit text passages (grammar checking, abridgements, translations, improvements to wording), I used prompts following this example:
   a. "Please rewrite this text to improve its flow, readability, and clarity while keeping the original information intact. Don't add, remove or change any facts, arguments, or meanings. Only rephrase sentences where needed for better coherence and readability. If something is already clear, leave it unchanged: [TEXT]"

2. To edit and generate Python code (speed up or improving existing code, automation, introduction of new functions, giving examples, debug), I used prompts following this example:
   a. "Is there a way to change this code, such that it doesn't safe the selected images in a dictionary but in an eeImageCollection and would this option be faster?"
   b. "I'm getting the following error in my code: "EEException: Error in map(ID=20191103T024849_20191103T030751_T49MEV): Number.lt: Parameter 'left' is required and may not be null.". Can you help me to find the cause?"

3. To search new articles or sources that weren't found with the usual search engines, I used prompts following this example (only in Consensus):
   a. "When does research say effects of reforestation can be detected using remotely sensed data?"

With my signature I confirm that the information provided above is true and accurate.

Date, Place
30.11.2025, Wil SG

Signature
U. Wittingau

# A. Appendix – Additional Material and Figures


**Figure A. 1:** Map with one example for each of the three land-cover types. One can clearly see the different structures of each land-cover type. While the Natural Forest and the Oil-Palm Plantation example are representative for how all sample sites look like, the agroforestry sample sites are more diverse.

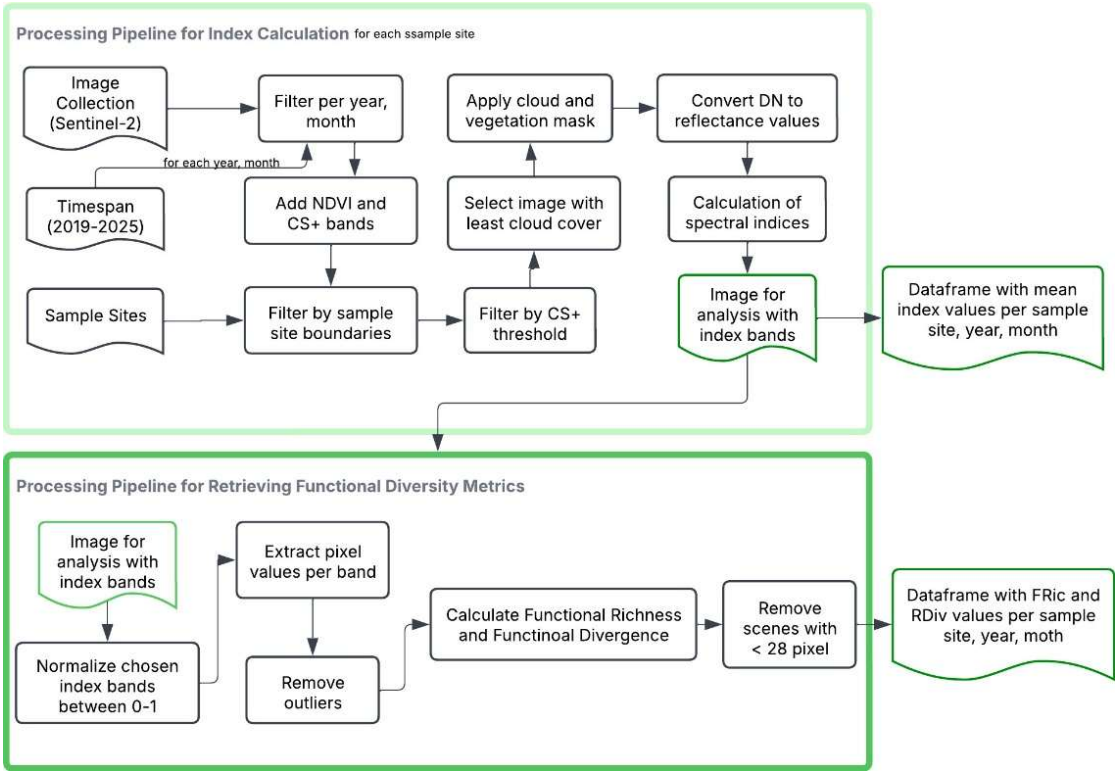


**Figure A. 2:** Schematic depiction of processing pipelines to calculate the spectral index values and the functional diversity metrics.

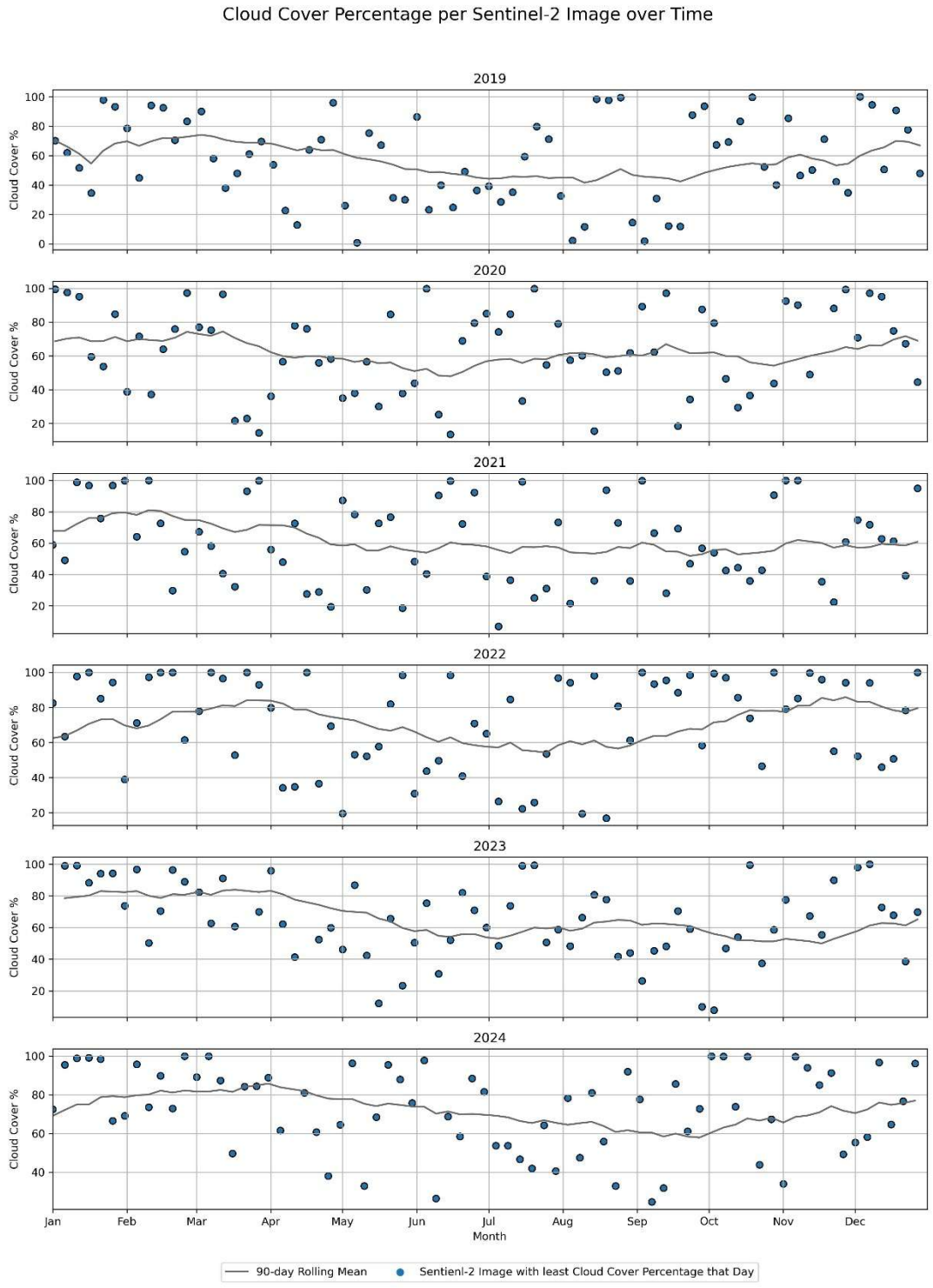


**Figure A. 3:** Sentine-2 images with their respective cloud cover percentage over the whole timespan of analysis that overlap with the sample sites. All sample sites were considered for this plot.

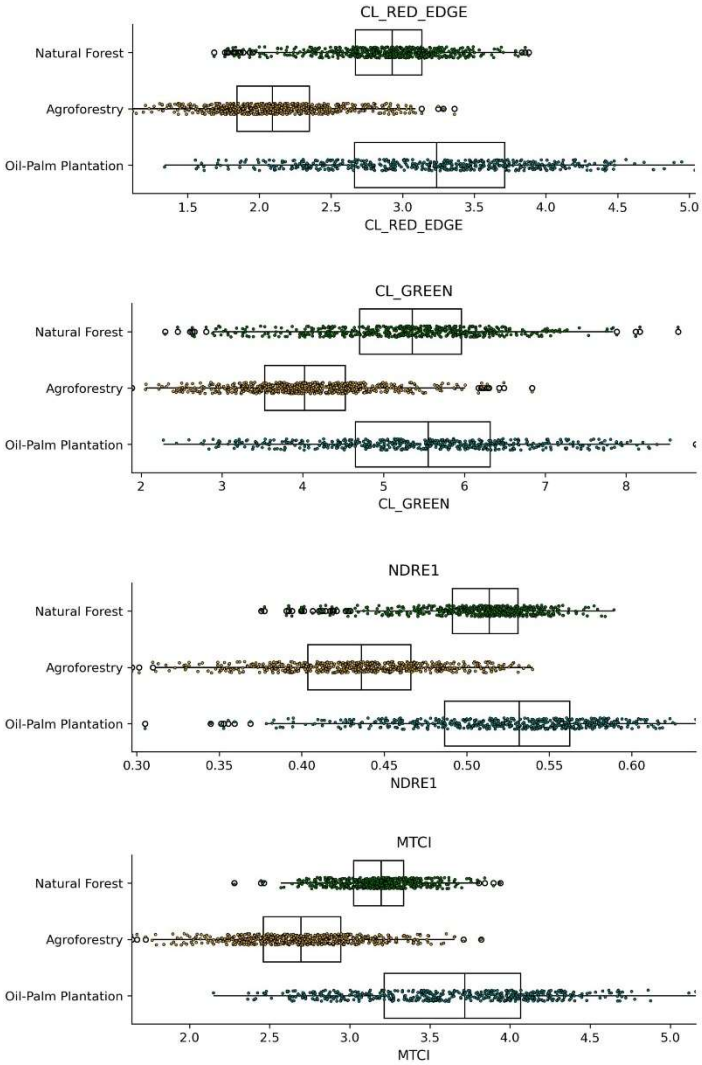


**Figure A. 4:** *:* Boxplots of Cl_red-edge, $Cl_{green}$, NDRE1 and MTCI

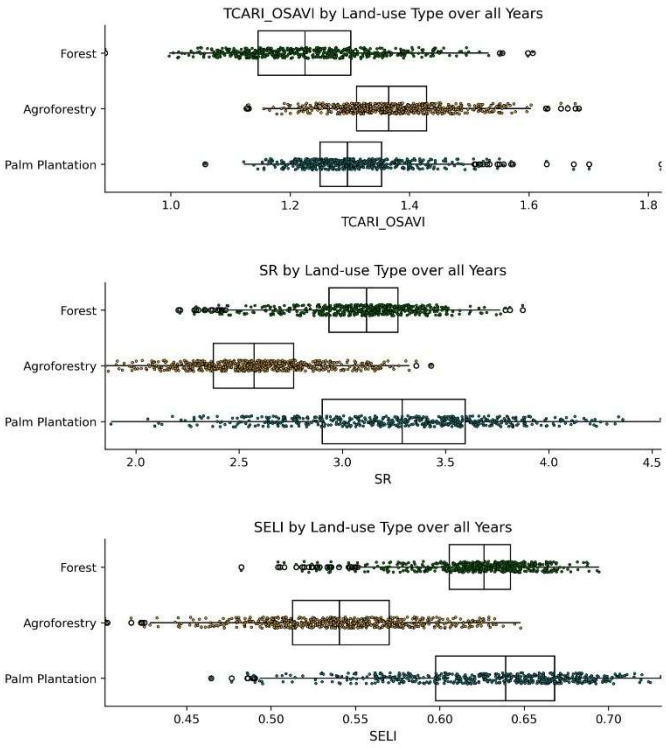


**Figure A. 5:** *:* Boxplots of TCARI/OSAVI, SR and SELI

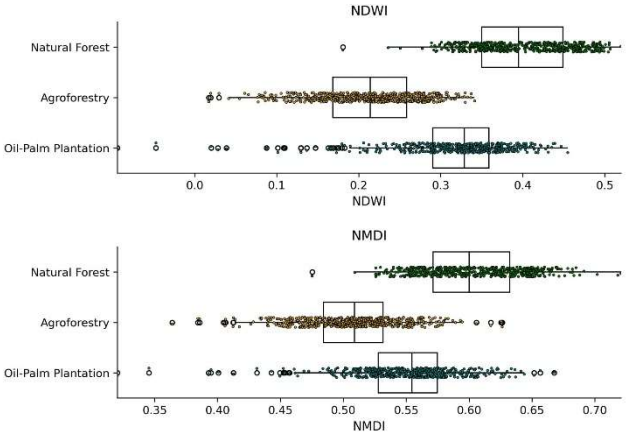


**Figure A. 6:** *:* Boxplots of NDWI and NMDI

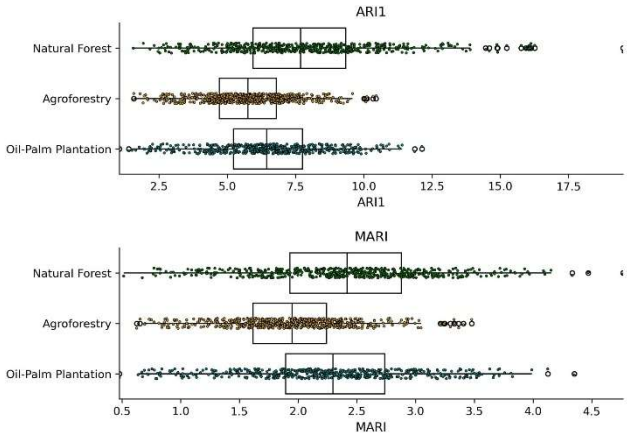


**Figure A. 7:** : Boxplots of ARI1 and mARI

**Table A. 1**: Indices with their respective categories and the Pearson r and p-values for their correlation with the CS+ medians of the sample sites.

| **Index Name** | **Category** | **Kruskal H-value** | **Kruskal p-value** |
|---|---|---|---|
| MTCI | Chlorophyll | -0.033 | 0.1820 |
| MSI | Water | -0.049 | 0.0503 |
| NDWI | Water | -0.062 | 0.0129 |
| NDII | Water | -0.062 | 0.0125 |
| OSAVI | Greenness | 0.090 | 0.0003 |
| NMDI | Water | -0.132 | 1.05E-07 |
| NDRE2 | Chlorophyll | 0.139 | 2.17E-08 |
| SELi | Stucture | 0.140 | 1.68E-08 |
| $CL_{red\text{-}edge}$ | Chlorophyll | 0.148 | 2.61E-09 |
| NDRE1 | Chlorophyll | 0.169 | 7.94E-12 |
| SR | Chlorophyll | 0.179 | 4.45E-13 |
| NDVI | Greenness | 0.277 | 8.29E-30 |
| EVI | Greenness | -0.310 | 2.93E-37 |
| $CL_{green}$ | Chlorophyll | 0.342 | 2.73E-45 |
| TCARI/OSAVI | Chlorophyll | -0.346 | 2.18E-46 |
| PSRI | Pigment | 0.378 | 9.61E-56 |
| mARI | Pigment | 0.476 | 1.13E-91 |
| ARI1 | Pigment | 0.533 | 1.17E-118 |
| CRI1 | Pigment | 0.548 | 5.20E-127 |